

# 1 Parallel Expansion and Divergence of the Hyr/Iff- 2 like (Hil) Adhesin Family in Pathogenic Yeasts 3 Including *Candida auris*

4 Rachel Smoak<sup>\*1</sup>, Lindsey F. Snyder<sup>\*2</sup>, Jan S. Fassler<sup>^3</sup>, Bin Z. He<sup>^3</sup>

5

6 <sup>1</sup>Civil and Environmental Engineering, <sup>2</sup>Interdisciplinary Graduate Program in Genetics, <sup>3</sup>Biology  
7 Department, University of Iowa, Iowa City, IA 52242

8 \*These authors contributed equally

9 ^Correspondence should be addressed to:

10 Bin Z. He, [bin-he@uiowa.edu](mailto:bin-he@uiowa.edu)

11 Jan S. Fassler: [jan-fassler@uiowa.edu](mailto:jan-fassler@uiowa.edu)

## 12 **Abstract**

13 Opportunistic yeast pathogens evolved multiple times in the Saccharomycetes class. A recent  
14 example is *Candida auris*, a multidrug resistant pathogen associated with a high mortality rate  
15 and multiple hospital outbreaks. Genomic changes shared between independently evolved  
16 pathogens could reveal key factors that enable them to infect the host. One such change may  
17 be the expansion of cell wall adhesins, which mediate biofilm formation and adherence and are  
18 established virulence factors in *Candida* spp. Here we show that homologs of a known adhesin  
19 family in *C. albicans*, the Hyr/Iff-like (Hil) family, repeatedly expanded in divergent pathogenic  
20 *Candida* lineages including in *C. auris*. Evolutionary analyses reveal varying levels of selective  
21 constraint and a potential role of positive selection acting on the ligand-binding domain during  
22 the family expansion in *C. auris*. The repeat-rich central domain evolved rapidly after gene  
23 duplication, leading to large variation in protein length and  $\beta$ -aggregation potential, both known  
24 to directly affect adhesive functions. Within *C. auris*, isolates from the less virulent Clade II lost  
25 five of the eight Hil homologs, while other clades show abundant tandem repeat copy number  
26 variation. We hypothesize that expansion and diversification of adhesin gene families are a key  
27 step towards the evolution of fungal pathogens and that variation in the adhesin repertoire could  
28 contribute to within and between species differences in the adhesive and virulence properties.

## 29 Introduction

30 *Candida auris* is a newly emerged multidrug-resistant yeast pathogen. It is associated with a  
31 high mortality rate – up to 60% in a multi-continent meta-analysis (Lockhart et al. 2017) – and  
32 has caused multiple outbreaks (CDC global *C. auris* cases count, February 15th, 2021). As a  
33 result, it became the first fungal pathogen to be designated by CDC as an urgent threat (CDC  
34 2019). The evolutionary origin of *C. auris* as a pathogen is part of a bigger evolutionary puzzle:  
35 *C. auris* belongs to a polyphyletic group known by the genus name of *Candida*, which contains  
36 most of the human yeast pathogens. Phylogenetically, however, species like *C. albicans*, *C.*  
37 *auris* and *C. glabrata* belong to distinct clades with close relatives that are not or rarely found to  
38 infect humans (Fig 1A). This strongly suggests that the ability to infect humans has evolved  
39 multiple times in yeasts (Gabaldón et al. 2016). As many of the newly emerged *Candida*  
40 pathogens are resistant or can quickly evolve resistance to antifungal drugs (Lamoth et al. 2018;  
41 Srivastava et al. 2018), it is urgent to understand how yeast pathogens arose and what make  
42 them better at surviving in the host. We reason that any shared genetic changes or biological  
43 processes affected among independently derived *Candida* pathogens could reveal key factors  
44 for host adaptation and could lead to new prevention and treatment strategies.

45 Gene duplications and the subsequent functional and regulatory changes are a major  
46 driver in evolution (Zhang 2003; Qian and Zhang 2014; Eberlein et al. 2017). For example, this  
47 mechanism was found to underlie the independent origin of digestive RNases in Asian and  
48 African leaf monkeys (Zhang 2006), as well as the ability of insects to feed on plants that  
49 produce toxic cardenolides (Zhen et al. 2012). In support of a key role for gene duplication and  
50 sequence divergence in the emergence of yeast pathogens, a genome comparison of six  
51 *Candida* species and related low-pathogenic potential species identified a list of pathogen-  
52 enriched gene families (Butler et al. 2009). Among the top six families, three are GPI-anchored  
53 cell wall proteins – Hyr/Iff-like, Als-like and Pga30-like – that are known or suggested to act as  
54 fungal adhesins. These heavily glycosylated cell wall proteins typically have a ligand-binding  
55 domain at the N-terminus, followed by a central domain rich in tandem repeats (Fig 1B). They  
56 play key roles in adhesion to host epithelial cells, biofilm formation and iron acquisition, and are  
57 well-established virulence factors (de Groot et al. 2013; Lipke 2018). It has been suggested that  
58 expansion of cell wall protein families, particularly adhesins, is a key step towards the evolution  
59 of yeast pathogens (Gabaldón et al. 2016). This is supported by a study showing that several  
60 adhesin families independently expanded in pathogenic *Candida* species within the  
61 *Nakaseomyces* genus (Gabaldón et al. 2013).

62           Despite the importance of adhesins in both the evolution and virulence of *Candida*  
63 pathogens, few studies have examined their evolutionary history, sequence divergence and the  
64 role of natural selection in pathogenic yeast species (Linder and Gustafsson 2008). In particular,  
65 little is known about adhesin genes in *C. auris* and their evolutionary relationship with homologs  
66 in other *Candida* species (Kean et al. 2018; Singh et al. 2019; Muñoz et al. 2021). Our goal in  
67 this study is to characterize and examine the evolutionary history and sequence divergence of  
68 adhesin genes in *C. auris* (Fig 1C, D). To identify candidate adhesins in *C. auris*, we draw on *C.*  
69 *albicans*, which belongs to the same CUG-Ser1 clade. Among known adhesins in *C. albicans*  
70 (Fig 1C), *C. auris* lacks the Hwp family and has only three Als or Als-like proteins, many fewer  
71 than the eight Als proteins in *C. albicans* (Fig 2A) (Muñoz et al. 2018). By contrast, *C. auris* has  
72 eight genes with a Hyphal\_reg\_CWP (PF11765) domain found in the Hyr/Iff family in *C. albicans*  
73 (Muñoz et al. 2021). This family was one of the most highly enriched in pathogenic *Candida*  
74 species relative to the non-pathogenic ones (Butler et al. 2009). Furthermore, transcriptomic  
75 studies identified two *C. auris* Hyr/Iff-like (Hil) genes as being upregulated during biofilm  
76 formation and under antifungal treatment (Kean et al. 2018). Interestingly, isolates from the less  
77 virulent *C. auris* Clade II lack five of the eight Hil genes (Muñoz et al. 2021). It is currently not  
78 known whether the *C. auris* Hil genes encode adhesins, how they relate to the *C. albicans*  
79 Hyr/Iff family genes and how their sequences diverged after duplication. We show in this study  
80 that the Hil family has convergently expanded in *C. auris* and *C. albicans* as well as in other  
81 pathogenic *Candida* species. Sequence features and predicted effector domain structure  
82 support the majority of the yeast Hil family, including all eight members in *C. auris*, as encoding  
83 adhesins. Evolutionary analyses reveal varying levels of selective constraint and a possible role  
84 of positive selection acting on the effector domain, while rapid divergence in the repeat-rich  
85 central domain leads to large variation in length and  $\beta$ -aggregation potential that could affect the  
86 adhesive properties of the yeast cells and thus generates phenotypic diversity.

## 87 **Results**

### 88 **Parallel expansion of the Hyr/Iff-like family in multiple pathogenic *Candida* lineages**

89 The Hyr/Iff family was first identified and characterized in *Candida albicans* (Bailey et al. 1996;  
90 Richard and Plaine 2007). A defining feature of the family is its ligand-binding domain, known as  
91 Hyphal\_reg\_CWP (PF11765), at the N-terminus. It is followed by a variable central domain rich  
92 in tandem repeats (Boisramé et al. 2011). In a previous study, Butler *et al* used “Hyr/Iff-like” to  
93 refer to any gene sharing sequence homology in either the ligand-binding domain or the repeat  
94 domain with the Hyr/Iff genes in *C. albicans* (Butler et al. 2009). In this study we restrict the

95 Hyr/Iff-like (Hil) family as referring to the group of evolutionarily related proteins containing the  
96 Hyphal\_reg\_CWP domain at the N-terminus, thus requiring both the presence of the ligand-  
97 binding domain and also conservation of its relative position in the protein.

98 We identified a total of 104 Hil family homologs from 18 species in the Saccharomycetes  
99 class (Table S1). No credible hits were identified outside of Saccharomycetes, suggesting that  
100 this family is likely specific to the yeast. Notably we didn't identify any homolog in the well-  
101 studied *S. cerevisiae* or its close relatives. Although the Pfam database does contains two *S.*  
102 *cerevisiae* proteins in the PF11765 domain family, we found that these two proteins are not only  
103 more divergent from those in *C. auris* than homologs in the equally distant *C. glabrata*, but also  
104 have a different domain organization, with their PF11765 domains in the middle rather than at  
105 the N-terminus of the proteins (Fig S1).

106 To infer the evolutionary history of the Hil family, especially the history of duplications  
107 among independently evolved *Candida* pathogens, we reconstructed a phylogenetic tree based  
108 on the PF11765 domain (Fig. 2B). We found that homologs from the Clavispora and Candida  
109 genera, which include *C. auris* and *C. albicans*, respectively, formed their own groups. This  
110 suggests that the duplications in the Hil families in the two clades occurred independently. To  
111 infer the timing of the duplication and loss events, we reconciled the PF11765 domain tree with  
112 the species tree (Materials and Methods). The result suggests a duplication at the root of the  
113 CUG-Ser1 clade, followed by repeated, parallel duplications in the Candida and Clavispora  
114 genera (Fig 2C). To highlight the uneven distribution of duplications among species, we inferred  
115 the number of gains and losses on each branch in the species tree, which shows the extensive  
116 and parallel expansion of the Hil family particularly in the *albicans* and the MDR clades (Fig 2D).  
117 In the literature the *C. auris* Hil family genes have been referred to by their most closely related  
118 Hyr/Iff genes in *C. albicans* (Kean et al. 2018; Jenull et al. 2021; Muñoz et al. 2021). To avoid  
119 the incorrect implication of one-to-one orthology between the *HIL* genes in the two species, we  
120 renamed the *C. auris* Hil family genes as Hil1-Hil8 ordered by their protein length (Table S2).

## 121 **Sequence features and predicted effector domain structure support *C. auris* Hil family as** 122 **adhesins**

123 Determining the adhesin status of the Hil family is important for understanding the implications  
124 of its parallel expansions. Experimental studies supported 11 of the 12 members of the Hil  
125 family proteins in *C. albicans* as adhesins (Bailey et al. 1996; Boisramé et al. 2011; Rosiana et  
126 al. 2021). Here we provide bioinformatic evidence supporting an adhesin function for all eight Hil  
127 proteins in *C. auris*. We take advantage of the characteristic domain architecture in known yeast  
128 adhesins, which consist of an N-terminal signal peptide, a ligand-binding (effector) domain, a



129 Ser/Thr-rich central domain with tandem repeats and  $\beta$ -aggregation prone sequences, and a  
130 Glycosylphosphatidylinositol (GPI) anchor at the C-terminus (Fig 3A) (de Groot et al. 2013;  
131 Lipke 2018). All eight *C. auris* Hil proteins share this domain architecture (Fig 3B) and have  
132 elevated Ser/Thr frequencies compared with the genome-wide distribution (Fig S2,3). All eight  
133 members were also predicted to be fungal adhesins by FungalRV, a support vector machine  
134 based classifier using amino acid composition and hydrophobic properties as input and showing  
135 high sensitivity and specificity in eight pathogenic fungi (Chaudhuri et al. 2011).

136 The structure of the effector domain in several yeast adhesin families, such as the Als,  
137 Epa and Flo families, have been solved and reveal a carbohydrate or peptide binding activity  
138 (Willaert 2018). Since an experimentally determined structure is not available for the PF11765  
139 effector domain, we used the recently released AlphaFold2 (Jumper et al. 2021) to predict the  
140 structures of the PF11765 domains in *C. auris* Hil1 and Hil7. We chose these two because the  
141 PF11765 domain in Hil1 is representative of 6 of the 8 Hil proteins while Hil7's is the least  
142 similar in sequence to the rest (Fig S4). Both predicted structures are of high confidence and  
143 adopt a highly similar  $\beta$ -solenoid fold, i.e., a superhelical arrangement of repeating  $\beta$ -strands  
144 around a central axis, stacked into an elongated cylinder (Fig 3C, D). The  $\beta$ -strand-rich nature is  
145 consistent with the structurally characterized yeast adhesin effector domains, although most of  
146 them have a different,  $\beta$ -sandwich fold (Willaert 2018). To understand the potential function of  
147 the PF11765 domain, we searched for similar structures with known functions using the  
148 threading-based prediction server, I-TASSER (Zhang 2008). I-TASSER identified templates with  
149 good structural alignment (normalized z-scores between 1 and 2) but low sequence identity (<  
150 20%). Remarkably, five of the six unique PDB structures in the top 10 list are from the binding  
151 domains of bacterial adhesins, such as the Serine-Rich Repeat Proteins (SRRPs) from *L.*  
152 *reuteri* (Fig 3E, Table 1 & S3) (Sequeira et al. 2018). Originally no yeast hits were found. This  
153 changed when a new study reported the same  $\beta$ -solenoid fold for two Adhesin-like wall proteins  
154 (Awp)'s effector domain from *C. glabrata* (PDB: 7O9Q, 7O9O/7O9P), which do not encode the  
155 PF11765 domain (Reithofer et al. 2021). Together, these results strongly support the ligand-  
156 binding activities for the PF11765 domain and the Hil proteins in *C. auris* as adhesins. The low  
157 sequence identity between the PF11765 domain, the bacterial adhesin binding regions and the  
158 *C. glabrata* Awp's effector domain further suggests that bacterial and yeast adhesins have  
159 convergently evolved towards a similar structure to achieve adhesion functions.

#### 160 **Diverged central domain may affect the adhesion function of the Hil proteins in *C. auris***

161 While the overall domain architecture is well conserved, the eight Hil family paralogs in *C. auris*  
162 differ significantly in length and sequence in their central domains. While the latter is not

163 involved in ligand binding, they nonetheless play critical roles in mediating adhesion. The length  
164 and stiffness of the central domain are essential for elevating and exposing the effector domain  
165 (Frieman et al. 2002; Boisramé et al. 2011). Moreover, they typically encode tandem repeats  
166 and  $\beta$ -aggregation sequences, which directly contribute to adhesion by mediating homophilic  
167 binding and amyloid formation (Rauceo et al. 2006; Otoo et al. 2008; Frank et al. 2010; Wilkins  
168 et al. 2018). Hence divergence in the central domain properties has the potential to generate  
169 functional diversity, as shown in *S. cerevisiae* (Verstrepen et al. 2004; Verstrepen et al. 2005).

170 To determine how the central domain sequences evolved in the *C. auris* Hil family, we  
171 used dot plots to examine their similarity. We found *C. auris* Hil1 to Hil4 share a ~44 aa repeat  
172 unit, whose copy number varies from 15 to 46, which drives their difference in length (Fig 4A).  
173 Hil7 and Hil8 encode the same repeat unit but has only one copy (Fig 4B, C). By contrast, Hil5  
174 and Hil6 encode very different, low complexity repeats with a period of 5-9 aa and between 14  
175 to 49 copies (Fig 4D, E). These variation also affected the Ser/Thr frequencies (Fig S2).

176 In addition to protein length and Ser/Thr frequencies, the tandem repeat evolution also  
177 leads to differences in the  $\beta$ -aggregation potential by altering the number and quality of  $\beta$ -  
178 aggregation prone sequences. Most characterized yeast adhesins contain 1-3 such sequences  
179 at a cutoff of >30%  $\beta$ -aggregation potential predicted by TANGO (Fernandez-Escamilla et al.  
180 2004; Ramsook et al. 2010; Lipke 2018). In *C. auris* Hil1 through Hil4, however, the shared ~44  
181 aa tandem repeat unit contains a heptapeptide (“GVVIVTT” and its variants) that is predicted to  
182 have >90%  $\beta$ -aggregation potential. As a result, the central domains of these proteins contain  
183 21 to 50 highly  $\beta$ -aggregation-prone sequences (e.g., Hil1 shown in Fig S5). We hypothesize  
184 that the unusually high number of  $\beta$ -aggregation sequences in Hil1-4 and the large variation  
185 among the *C. auris* Hil proteins – only 2-4 were identified in Hil5-Hil8 – lead to diverse adhesion  
186 functions within the *C. auris* Hil family.

### 187 **Intraspecific variation in Hil family size and tandem repeat copy number in *C. auris* could** 188 **drive phenotypic diversity in adhesion and virulence**

189 *C. auris* isolates from geographically and genetically divergent clades contain varying numbers  
190 of Hil family homologs (Muñoz et al. 2021). In particular, strains from the East Asian Clade, or  
191 Clade II, have only three of the eight members, while most strains from the other clades have  
192 eight (Muñoz et al. 2021). Our phylogenetic analysis shows that clade II strains lost Hil1-Hil4  
193 and Hil6 (Fig S6). Clade II strains also lack seven of the eight members of another GPI-anchor  
194 family that is specific to *C. auris* (Muñoz et al. 2021). Together, these suggest that clade II  
195 strains may have reduced adhesive capability. Interestingly, this lack of putative adhesins in  
196 Clade II coincide with the observation that >93% of Clade II isolates described in a study were

197 associated with ear infections in contrast to invasive infections and hospital outbreaks typically  
198 caused by the other clades, and they also appear to be less resistant to antifungals (Kwon et al.  
199 2019; Welsh et al. 2019).

200 Tandem repeats are prone to recombination-mediated expansions and contractions,  
201 which in turn can contribute to diversity in cell adhesive properties, as shown in *S. cerevisiae*  
202 (Verstrepen et al. 2005). Sampling nine strains in *C. auris*, we observed clade-specific variation  
203 in tandem repeat copy number in Hil1-Hil4 (Table 2). Except for one 16 aa deletion affecting one  
204 strain, all seven remaining indels correspond to one or multiples of a full repeat, consistent with  
205 their being driven by recombination between repeats (Fig S7).

### 206 **Natural selection on the effector domain and the tandem repeats in *C. auris* Hil genes**

207 Gene duplication is often followed by a period of relaxed functional constraints on one or both  
208 copies, allowing for sub- or neo-functionalization (Zhang 2003; Innan and Kondrashov 2010). If  
209 positive selection is involved, it can lead to an elevated ratio of nonsynonymous to synonymous  
210 substitution rates  $dN/dS > 1$  (Yang 1998). Here we ask if the ligand binding (PF11765) domain  
211 in *C. auris* Hil1-Hil8 showed any signature of positive selection during the Hil family expansion.

212 We first tested the hypothesis that the PF11765 domain has evolved under a constant  
213 selection strength during the expansion of the Hil family in *C. auris*. A likelihood ratio test (LRT)  
214 comparing the one-ratio model (constant selection) with the free-ratio model (varying selection  
215 at each branch) is highly significant ( $2\Delta l = 446.68$ ,  $P < 10^{-10}$  for  $X^2$  with d.f. = 13). This suggests  
216 that selection strengths vary among lineages. The free-ratio model identified two branches with  
217 a  $dN/dS$  ratio far greater than one ( $\omega_1$ , 2 in Fig 5A). We tested if one or both have significantly  
218 higher  $dN/dS$  than the other branches (tests a, b and c in Table 3). The LRT results supported  
219 all three hypotheses, either tested together (a) or separately (b and c). We further asked if their  
220  $dN/dS$  ratios are significantly greater than 1 (tests d, e and f in Table 3). Only the test with the  
221 two branches combined is significant at a 0.05 level. Two more branches showed elevated  
222  $dN/dS$  ratios that are close to or just above 1 under the free-ratio model (labeled  $\omega_3$  in Fig 5).  
223 LRT supports them being significantly different from the background  $dN/dS$  (test g, Table 3).  
224 Our results thus identified four branches with significantly elevated  $dN/dS$  over the background,  
225 with two of them showing modest evidence for  $dN/dS > 1$ , consistent with positive selection  
226 acting on the PF11765 domain. Overall, we conclude that expansion of the Hil family in *C. auris*  
227 was accompanied by relaxation of selective constraints on the PF11765 domain and may have  
228 involved episodes of positive selection driving functional divergence.

229 We showed previously that the central domain, especially the tandem repeats therein,  
230 evolved rapidly within the *C. auris* Hil family. Given their potential to affect the adhesin functions,

231 we ask what types of selective forces govern the evolution of the tandem repeats. Hil1 and Hil2  
232 duplicated recently in *C. auris* (Fig S6) and their repeats have a conserved 44 aa period (Table  
233 2), allowing us to answer this question. Following a pioneer study by (Persi et al. 2016) on  
234 tandem repeat evolution, we estimated the pairwise dN/dS ratios between individual repeats  
235 within Hil1/Hil2 (termed “horizontal evolution”) and compared them to the estimates between the  
236 repeats across the two proteins (“vertical evolution”, Fig 5B). Phylogenetic tree for the repeats  
237 suggests that most of the repeats in Hil1 and Hil2 either originated after gene duplication or  
238 were subject to homogenization by gene conversion (Fig 5C). As a result, orthology between  
239 the repeats across genes is limited and difficult to determine. Thus, we inferred the selective  
240 strength for vertical evolution using pairwise dN/dS estimates between a set of 17 repeats from  
241 each of Hil1 and Hil2 (cyan lines, Fig 5B). As an alternative approach, we assumed a relatively  
242 well-aligned part of the tandem repeat region is orthologous and estimated dN/dS based on that  
243 (yellow region, Fig 5B). Both approaches yielded similar results: the distributions of dN/dS ratios  
244 within Hil1 or Hil2 are similar to each other (Fig 5D, Wilcoxon Rank Sum Test  $P = 0.10$ ), and are  
245 significantly different (lower) than that for the inter-Hil1-Hil2 repeats (Wilcoxon Rank Sum Test  $P$   
246  $< 0.01$ ). This suggest that after gene duplication, the repeats in one or both copies were under  
247 relaxed constraint or possibly positive selection, which allowed them to diverge between the two  
248 genes. Afterwards, there was increased constraint in each gene to maintain the repeats within a  
249 gene. The dN/dS ratios of the repeats either within or between the two genes are higher than  
250 those obtained for the PF11765 domain between Hil1, Hil2 and closely related MDR homologs  
251 (Fig 5D), suggesting that the repeats in general evolved under weaker selective constraint than  
252 did the PF11765 domain.

### 253 **The yeast Hil family has adhesin-like domain architecture with rapidly diverging central** 254 **domain sequences**

255 Above we focused on the Hil family in *C. auris* and provided a detailed picture of the adhesin  
256 features and sequence divergence after duplication. Here we apply these analyses to the entire  
257 Hil family in yeasts. We found that 92/104 homologs were predicted to be fungal adhesins by  
258 FungalRV, and 97 and 89 were predicted to have a signal peptide and GPI-anchor, respectively  
259 (Fig S8A), consistent with most of the yeast adhesins being GPI-anchored cell wall proteins  
260 (Lipke 2018). 76 of the 104 Hil homologs passed all three tests. Moreover, all but five homologs  
261 encode tandem repeats in their central domain, with proteins longer than 1500 aa having a  
262 significantly higher proportion of their central domain consisting of tandem repeats (Fig S8B). Hil  
263 homologs also have a higher serine and threonine content compared with the proteome-wide  
264 distribution (Fig S8C). All of them have at least one  $\beta$ -aggregation prone sequence. Finally,

265 structural predictions for the PF11765 domain in three Hil proteins from *C. albicans*, *C. glabrata*  
266 and *K. lactis* all showed a similar  $\beta$ -solenoid fold as predicted for *C. auris* Hil1 and Hil7 and  
267 shared with the bacterial SRRP adhesins (Fig S9). Together, these lines of evidence suggest  
268 that the majority of the yeast Hil family encode fungal adhesins.

269         Similar to our findings in *C. auris*, the yeast Hil family as a whole exhibits large variation  
270 in protein length and sequence properties within their central domain (Fig 6). For protein length,  
271 the non-PF11765 portion of these proteins have a mean and standard deviation of  $936.8 \pm 725.1$   
272 aa and a median of 650.5 aa (Fig 6A). This variation in protein length is almost entirely driven by  
273 the tandem repeats (Fig 6B, linear regression slope = 0.996,  $r^2 = 0.76$ ). Not only do the tandem  
274 repeats vary in copy number, but the underlying sequences also diverged rapidly (Fig S10,  
275 Table S4). This leads to large variation in sequence properties such as  $\beta$ -aggregation potential  
276 (Fig 6C). A subset of Hil homologs consisting of *C. auris* Hil1-4 and their closely related proteins  
277 in the MDR clade are unique even within the family: they are longer than the other Hil homologs  
278 (1592 vs. 918.5 aa in median length) and also have more TANGO positive motifs (22 vs 4 in  
279 median number of total hits). A curious and distinct feature of the TANGO motifs in this group is  
280 that they are regularly spaced as a result of the motif being part of the repeat (median absolute  
281 deviation, or MAD, of distances between adjacent strong TANGO “hits” less than 5 aa, Fig. 6D).  
282 The heptapeptide “GVVIVTT” and its variants account for 61% of all hits in this subset and are  
283 not found in the other Hil homologs (Table S5).

#### 284 **The yeast Hil family genes are preferentially located near chromosome ends**

285 Several well-characterized yeast adhesin families, such as the Epa family in *C. glabrata* and the  
286 Flo family in *S. cerevisiae*, are enriched in the subtelomeres (Teunissen and Steensma 1995;  
287 De Las Peñas et al. 2003). This region is associated with high rates of SNPs, indels and copy  
288 number variations, and can undergo ectopic recombination that can lead to the spread of genes  
289 between chromosome ends or their losses (Mefford and Trask 2002; Anderson et al. 2015). We  
290 found that the yeast Hil family genes are frequently located near the chromosome ends as well  
291 (Fig S11). To test if this trend is significant, we compared their chromosomal locations with the  
292 background gene density distribution in six species whose genomes are assembled to a  
293 chromosomal level (Table S6, Materials and Methods). We found the Hil family genes are  
294 indeed enriched at the chromosome ends (Fig. 7A, B). A goodness-of-fit test confirmed that the  
295 difference between the distribution of chromosomal locations of the Hil family and the genome  
296 background is significant ( $P = 3.6 \times 10^{-6}$ ). It has been shown that ectopic recombination between  
297 subtelomeres can lead to the spread and amplification of gene families (Anderson et al. 2015).



298 We thus hypothesize that the enrichment of the Hil family towards the chromosome ends is both  
299 a cause and consequence of its parallel expansion in different *Candida* lineages (Fig 7C).

## 300 Discussion

301 Yeast adhesin families were among the most enriched gene families in pathogenic lineages  
302 relative to the low pathogenic potential relatives (Butler et al. 2009). It has been proposed that  
303 expansion of adhesin families could be a key step in the emergence of novel yeast pathogens  
304 (Gabaldón et al. 2016). However, detailed phylogenetic studies supporting this hypothesis are  
305 rare (Gabaldón et al. 2013), and far less is known about how their sequences diverge and what  
306 selective forces are involved during the expansions. In this study, we resolved a detailed  
307 evolutionary history for the Hyr/Iff-like (Hil) family and characterized its sequence divergence  
308 and the selection forces involved. Our results support the previous finding that adhesin families  
309 are enriched in pathogenic yeasts (Fig 2A). Phylogenetic analysis convincingly showed that this  
310 correlation resulted from convergent expansions, with most of the duplications occurring in the  
311 *albicans* clade and the Multi-Drug Resistant (MDR) clade in two separate genera (Fig 2D).

312 The Hil family was experimentally studied in *C. albicans* (Bailey et al. 1996; Luo et al.  
313 2010; Boisramé et al. 2011), revealing 11 of its 12 members as GPI-anchored cell wall proteins  
314 with a potential role in adhesion. Similar evidence is lacking for family members in other yeasts.  
315 We showed that ~75% of all Hil proteins, including all eight members in *C. auris*, are predicted  
316 to be GPI-anchored cell wall proteins and pass a fungal adhesin predictor's (FungalRV) cutoff,  
317 supporting the adhesin status for the Hil family in general. We also used AlphaFold2 to make  
318 high-confidence predictions for the effector domain structure in several distantly related Hil  
319 proteins, all of which showed the same  $\beta$ -solenoid fold (Fig 3C-E, S8). This structure is highly  
320 similar to the binding region of some bacterial adhesins, e.g., the Serine Rich Repeat Protein  
321 (SRRP) in *L. reuteri* (Sequeira et al. 2018) as well as two newly reported yeast adhesin effector  
322 domains (Reithofer et al. 2021). The cross-kingdom similarity in the adhesin effector domain  
323 structure is intriguing in several ways. First, it suggests convergent evolution in bacteria and  
324 yeasts. Second, what's known about the structure-function relationship in bacteria can provide  
325 insight into the PF11765 domain in yeast. Notably, *LrSRRP* shows a pH-dependent substrate  
326 specificity that is potentially adapted to distinct host niches (Sequeira et al. 2018). Finally, the  
327 similar structure and function of the bacterial and yeast adhesins could mediate cross-kingdom  
328 interactions in natural and host environments (Uppuluri et al. 2018).

329 Sequence divergence after gene duplication allows for sub- or neo-functionalization that  
330 fuels evolution (Zhang 2003; Innan and Kondrashov 2010; Eberlein et al. 2017). Using *C. auris*



331 as a focal species, we found that while the PF11765 domain in its *HIL* genes evolved under  
332 purifying selection in general ( $dN/dS < 0.2$ ), four branches showed significantly higher  $dN/dS$   
333 ratios, including two with modest evidence for a  $dN/dS > 1$ , suggesting positive selection in  
334 addition to relaxed selective constraints (Fig 5A, Table 3). The implication is that changes in the  
335 effector domain sequence could affect the specificity or affinity for its substrates, which in turn  
336 could impact the adhesive properties of the cell. Experiments to characterize the binding affinity  
337 and substrate specificity of the eight Hil proteins in *C. auris* will be highly desired. Compared to  
338 the conserved effector domain, the central domain of the Hil family evolved much more rapidly  
339 after gene duplication, generating large variation in protein length and  $\beta$ -aggregation potential  
340 (Fig 3, 6). Evolutionary analyses comparing the repeat sequences in the recently duplicated Hil1  
341 and Hil2 showed that 1) the tandem repeats were also subject to purifying selection, albeit to a  
342 less extent than the PF11765 domain; 2) most of the repeats in the two genes likely originated  
343 after gene duplication, underscoring their dynamic nature; 3) the  $dN/dS$  ratios are slightly higher  
344 for repeats across the two genes than within each gene, consistent with a period of relaxed  
345 constraint after gene duplication. Although a role for positive selection cannot be ruled out.  
346 Together, our analyses painted a detailed evolutionary picture for how repeats originate, evolve  
347 and are selectively maintained.

348 Variations in protein length and  $\beta$ -aggregation potential resulting from the central domain  
349 divergence could directly impact the adhesion functions (Verstrepen et al. 2005; Alsteens et al.  
350 2010; Ramsook et al. 2010; Boisramé et al. 2011; Lipke et al. 2012). In this regard, we found *C.*  
351 *auris* Hil1-4 and the closely related MDR homologs to be unusual as they have as many as 50  
352  $\beta$ -aggregation prone sequences in contrast to 1-3 in known yeast adhesins (Ramsook et al.  
353 2010). This raises the question of whether they possess special adhesive properties. In addition  
354 to sequence divergence between homologs, we also identified intraspecific variation in the size  
355 and tandem repeat copy number of the Hil family. It has been shown previously that the Clade II  
356 strains in *C. auris* lack five of the eight Hil genes (Muñoz et al. 2021). We showed that this is  
357 due to gene loss (Fig S6). Interestingly, Clade II strains are unique among *C. auris* strains in  
358 that they are mostly associated with ear infections rather than hospital outbreaks as the other  
359 clades do (Kwon et al. 2019; Welsh et al. 2019). Since they also lack a *C. auris* specific GPI-  
360 anchored cell wall protein family (Muñoz et al. 2021), we hypothesize that Clade II strains have  
361 weaker adhesive abilities, which may be a cause or consequence of their distinct niche  
362 preference. We also found tandem repeat copy number variations in Hil1-Hil4 among clade I, III  
363 and IV strains in *C. auris*. As shown experimentally for the *S. cerevisiae* Flo family, adhesin  
364 protein length is strongly correlated with the adhesive properties and the flocculation and biofilm

365 formation capabilities (Verstrepen et al. 2005). Thus, Hil protein length variations in *C. auris*  
366 could further contribute to diversity in its adhesive properties and virulence.

367 Finally, we found that the Hil family genes are preferentially located near chromosomal  
368 ends in the species examined (Fig 7), similar to previous findings for the Flo and Epa families  
369 (Teunissen and Steensma 1995; De Las Peñas et al. 2003). This location bias can be both a  
370 cause and consequence of the family expansion, as it is known that subtelomeres are subject to  
371 ectopic recombination that can lead to the spread of gene families between chromosome ends  
372 (Mefford and Trask 2002; Anderson et al. 2015). In addition to a higher rate of gene gains and  
373 losses, there are two other consequences for the Hil family being located in the subtelomeres:  
374 1) the higher rates of mutations and structural variations associated with the subtelomeres could  
375 drive rapid diversification of the adhesin gene family (Snoek et al. 2014; Xu et al. 2021); 2) gene  
376 expression in the subtelomere is subject to epigenetic silencing, which can be derepressed in  
377 response to stress (Ai et al. 2002). Such epigenetic regulation of the adhesin genes was found  
378 to generate cell surface heterogeneity in *S. cerevisiae* and leads to hyperadherent phenotypes  
379 in *C. glabrata* (Halme et al. 2004; Castaño et al. 2005).

380 Together, our results provide a detailed phylogenetic analysis for a putative adhesin  
381 family in the Saccharomycetes, supporting the hypothesis that parallel expansions and the  
382 ensuing diversification of adhesins are a key step towards the evolution of yeast pathogens. Our  
383 results point to possible functional divergences between and within species in terms of adhesive  
384 properties, particularly in the emerging, multi-drug resistant species *C. auris*, which could have  
385 significant impact on their virulence profiles.

## 386 **Materials and Methods**

### 387 **RESOURCE AVAILABILITY**

#### 388 **Lead contact**

389 Further information and requests for resources and reagents should be directed to and will be  
390 fulfilled by the Lead Contact, Bin Z. He (bin-he@uiowa.edu).

#### 391 **Data and code availability**

392 All raw data and code for generating the intermediate and final results are available at the  
393 GitHub repository at <https://github.com/binhe-lab/C037-Cand-auris-adhesin>. Upon publication,  
394 this repository will be digitally archived with Zenodo and a DOI will be minted and provided to  
395 ensure reproducibility.

#### 396 **Software and algorithms list**

<b>NAME</b>	<b>REFERENCE</b>	<b>WEB OR DOWNLOAD URL</b>
FungalRV	(Chaudhuri et al. 2011)	<a href="http://fungalrv.igib.res.in/">http://fungalrv.igib.res.in/</a>
SignalP 5.0	(Almagro Armenteros et al. 2019)	<a href="http://www.cbs.dtu.dk/services/SignalP/">http://www.cbs.dtu.dk/services/SignalP/</a>
PredGPI	(Pierleoni et al. 2008)	<a href="http://gpcr.biocomp.unibo.it/pr-edgpi/">http://gpcr.biocomp.unibo.it/pr-edgpi/</a>
hmmscan	(Potter et al. 2018)	<a href="https://www.ebi.ac.uk/Tools/hmmer/search/hmmscan">https://www.ebi.ac.uk/Tools/hmmer/search/hmmscan</a>
XSTREAM	(Newman and Cooper 2007)	<a href="https://amnewmanlab.stanford.edu/xstream/download.jsp">https://amnewmanlab.stanford.edu/xstream/download.jsp</a>
EMBOSS v6.6.0.0	(Rice et al. 2000)	<a href="http://emboss.open-bio.org/">http://emboss.open-bio.org/</a>
TANGO v2.3.1	(Fernandez-Escamilla et al. 2004)	<a href="http://tango.crg.es/">http://tango.crg.es/</a>
JDotter	(Brodie et al. 2004)	<a href="https://4virology.net/virology-ca-tools/jdotter/">https://4virology.net/virology-ca-tools/jdotter/</a>
Clustal Omega v1.2.4	(Sievers et al. 2011)	<a href="http://www.clustal.org/omega/">http://www.clustal.org/omega/</a>
Jalview v2.11.1.4	(Waterhouse et al. 2009)	<a href="https://www.jalview.org/">https://www.jalview.org/</a>
BLAST+ v2.12.0	(Camacho et al. 2009)	<a href="https://blast.ncbi.nlm.nih.gov/">https://blast.ncbi.nlm.nih.gov/</a>
AlphaFold2	(Jumper et al. 2021)	<a href="https://github.com/sokrypton/ColabFold">https://github.com/sokrypton/ColabFold</a> (links to DeepMind Google Colab Notebook)
SwissModel	(Waterhouse et al. 2018)	<a href="https://swissmodel.expasy.org/">https://swissmodel.expasy.org/</a>
I-TASSER	(Zhang 2008)	<a href="https://zhanggrouop.org/I-TASSER/">https://zhanggrouop.org/I-TASSER/</a>
PyMol v2.5.2	(Schrödinger, LLC 2021)	<a href="https://pymol.org/">https://pymol.org/</a>
RAxML v8.2.12	(Stamatakis 2014)	<a href="https://cme.its.org/exelixis/web/software/raxml/">https://cme.its.org/exelixis/web/software/raxml/</a>
GeneRax v2.0.1	(Morel et al. 2020)	<a href="https://github.com/BenoitMorel/GeneRax">https://github.com/BenoitMorel/GeneRax</a>
FigTree v1.4.4	NA	<a href="http://tree.bio.ed.ac.uk/software">http://tree.bio.ed.ac.uk/software</a>

		<a href="#">e/figtree/</a>
Notung v2.9	(Chen et al. 2000)	<a href="http://www.cs.cmu.edu/~durand/Notung/">http://www.cs.cmu.edu/~durand/Notung/</a>
PAML v4.9e	(Yang 2007)	<a href="http://abacus.gene.ucl.ac.uk/software/paml.html">http://abacus.gene.ucl.ac.uk/software/paml.html</a>
bedtools v2.30.0	(Quinlan and Hall 2010)	<a href="https://bedtools.readthedocs.io/en/latest/index.html">https://bedtools.readthedocs.io/en/latest/index.html</a>
PAL2NAL.pl	(Suyama et al. 2006)	<a href="http://www.bork.embl.de/pal2nal/">http://www.bork.embl.de/pal2nal/</a>
R v4.1.0	(R Core Team)	<a href="https://cran.r-project.org/">https://cran.r-project.org/</a>
R package - ggtree v3.2.1	(Yu 2020)	<a href="https://github.com/YuLab-SMU/ggtree">https://github.com/YuLab-SMU/ggtree</a>
R package - treeio v1.18.1	(Wang et al. 2020)	<a href="https://github.com/YuLab-SMU/treeio">https://github.com/YuLab-SMU/treeio</a>
R package - rentrez v1.2.3	(Winter 2017)	<a href="https://github.com/ropensci/rentrez">https://github.com/ropensci/rentrez</a>
RStudio v1.4	(RStudio Team 2021)	<a href="https://www.rstudio.com/">https://www.rstudio.com/</a>
Custom R, Python and shell scripts	This study	<a href="https://github.com/binhe-lab/C037-Cand-auris-adhesin">https://github.com/binhe-lab/C037-Cand-auris-adhesin</a>

397

## 398 **METHOD DETAILS**

### 399 **Identify Hyr/Iff-like (Hil) family homologs in yeasts and beyond**

400 To identify the Hyr/Iff-like (Hil) proteins in *C. auris*, we used the Hyphal\_reg\_CWP domain from  
401 Hil1 of B11221 as the query and searched against the annotated protein sequences from the  
402 representative strains in Clade I to Clade IV (B8441, B11220, B11221, B11243) using blastp  
403 (v2.12.0, “-max\_hsp = 1”). To identify the Hil family proteins in yeasts and beyond, we used the  
404 same query as above and searched the RefSeq protein database with an E-value cutoff of  $1 \times 10^{-5}$ ,  
405 a minimum query coverage of 50% and with the low complexity filter on. All 189 hits were from  
406 Ascomycota (yeasts) and all but one were from the Saccharomycetes class (budding yeast). A  
407 single hit was found in the fission yeast *Schizosacchomyces cryophilus*. Using that hit as the  
408 query, we searched all fission yeasts in the nr protein database, with a relaxed E-value cutoff of  
409  $10^{-3}$  and identified no additional hits. We thus excluded that one hit from downstream analyses.  
410 We refined the remaining list of sequences by removing the following species, which were

411 already represented by well-studied relatives in the list: *Metschnikowia bicuspidata* var.  
412 *Bicuspidata*, *Debaryomyces fabryi*, *Suhomyces tanzawaensis*, *Candida orthopsilosis*,  
413 *Meyerozyma guilliermondii*, *Yamadazyma tenuis*, *Diutina rugosa*, *Kazachstania africana*,  
414 *Kazachstania naganishii*, *Naumovozyma dairenensis* and *Cyberlindnera jadinii*. We further  
415 excluded those that were 500 aa or shorter (notably the fission yeast hit is 339 aa). This was  
416 based on studies of the Epa family in *C. glabrata* and the Hyr/Iff family in *C. albicans* showing  
417 that a critical length is required for the adhesin function (Frieman et al. 2002; Boisramé et al.  
418 2011). The 27 sequences that were removed by the length criterion were primarily from two  
419 species: *C. parapsilosis* (10) and *S. stipitis* (12) (Table S7). In total 95 sequences were left after  
420 both filtering steps.

421         The RefSeq database lacks many yeast species such as those in the *Nakaseomyces*  
422 genus, which includes multiple *Candida* pathogens. We thus searched two additional yeast-  
423 specific databases: FungiDB (Basenko et al. 2018) and Genome Resources for Yeast  
424 Chromosomes (GRYC, <http://gryc.inra.fr/>). Using the same criteria, we recovered five and four  
425 additional sequences, resulting in a final dataset of 104 homologs from 18 species.

#### 426 **Phylogenetic analysis of the Hil family and inference of gene duplications and losses**

427 To infer the evolutionary history of the Hil family, which is characterized by its single effector  
428 domain, the PF11765 domain, we reconstructed a phylogenetic tree based on the alignment of  
429 that domain. First, the N-terminal 500 amino acid sequences for each Hil family protein were  
430 extracted, which included the PF11765 domain. These sequences were then aligned using  
431 Clustal Omega with the parameter `{--iter=5}`. The alignment was manually inspected and the  
432 first 480 columns were determined to contain the PF11765 domain and thus used for gene tree  
433 reconstructions. RAxML v8.2.12 was compiled and run on the University of Iowa ARGON server  
434 with the following parameters on the alignment: `"mpirun raxmlHPC-MPI-AVX -f a -x 12345 -p`  
435 `12345 -# 500 -m PROTGAMMAAUTO"`. The resulting tree was manually inspected in FigTree  
436 (v1.4.4). To infer the history of duplications and losses, the gene tree was reconciled with a  
437 species tree based on the literature (Muñoz et al. 2018; Shen et al. 2018) using Notung v2.9  
438 (Chen et al. 2000). To do so, the protein names in the gene tree were edited to include the  
439 species name as a postfix. In Notung, we first ran a rooting analysis which, in agreement with  
440 our expectation, identified the branch that separated the *Saccharomycetaceae* sequences from  
441 the CUG-Ser1 sequences as the best root choice. The reconciled tree was then rearranged with  
442 an edge weight threshold of 80.0, which allowed branches with less than 80% rapid  
443 bootstrapping support to be swapped. All rearrangements were ranked by the total event score,  
444 which is a weighted sum of penalties for duplications (1.5) and losses (1.0). The rearrangement

445 with the lowest total event score was chosen as the most likely tree. As the branch length  
446 values for the swapped branches were no longer meaningful, the final tree was represented as  
447 a cladogram. Tree annotation and visualization were done in R using the treeio and ggtree  
448 packages (Wang et al. 2020; Yu 2020).

449 To refine the phylogenetic tree for the Hil family in *C. auris* and infer gains and losses  
450 within the species, we identified orthologs of the Hil genes in representative strains of the four  
451 major clades of *C. auris* (B8441, B11220, B11221, B11243) (Muñoz et al. 2018). Orthologs from  
452 two MDR species, *C. haemuloni* and *C. pseudohaemulonis*, and an outgroup *D. hansenii* were  
453 also included. Gene tree was constructed as described above. To root the tree, we first inferred  
454 a gene tree without including the outgroup (*D. hansenii*) sequences in the alignment. Then the  
455 full alignment with the outgroup sequences along with the gene tree from the first step were  
456 provided to RAxML to run the Evolutionary Placement Algorithm (EPA) algorithm (Berger et al.  
457 2011), which identified a unique root location. To reconcile the gene tree with the species tree,  
458 we performed maximum likelihood based gene tree correction using GeneRax (v2.0.1) with the  
459 parameters: {--rec-model UndatedDL --max-spr-radius 5} (Morel et al. 2020). The inferred gene  
460 tree was used as the starting tree and a “species” tree that depicts the relationship between the  
461 strains of *C. auris* and the three other species was based on (Muñoz et al. 2018).

#### 462 **Prediction of adhesin-related sequence features**

463 **1)** Signal Peptide was predicted using the SignalP 5.0 server, with the “organism group” set to  
464 Eukarya (Almagro Armenteros et al. 2019). The server reported the proteins that had predicted  
465 signal peptides. No further filtering was done. **2)** GPI-anchor was predicted using PredGPI  
466 (Pierleoni et al. 2008) using the General Model. The server reports the false positive rate and  
467 predicted omega-site for each input protein. We defined proteins with a false positive rate of  
468 0.01 or less as containing a GPI-anchor. **3)** Pfam domains in each of the proteins, including the  
469 Hyphal\_reg\_CWP domain, were identified using the hmmscan (Potter et al. 2018). **4)** Tandem  
470 repeats were identified using XSTREAM (Newman and Cooper 2007) with the following  
471 parameters: {-i.7 -l.7 -g3 -e2 -L15 -z -Asub.txt -B -O}, where the “sub.txt” was provided by the  
472 software package. **5)** Serine and Threonine content in proteins were quantified using freak from  
473 the EMBOSS suite, using a sliding window of 100 aa, with a step size of 10 aa (Rice et al.  
474 2000). **6)**  $\beta$ -aggregation prone sequences were predicted using TANGO v2.3.1 with the  
475 following parameters: {ct="N" nt="N" ph="7.5" te="298" io="0.1" tf="0" stab="-10" conc="1"  
476 seq="SEQ"} (Fernandez-Escamilla et al. 2004). **7)** Lastly, FungalRV, a Support Vector Machine  
477 based fungal adhesin predictor, was used to evaluate all Hil family proteins (Chaudhuri et al.  
478 2011). Proteins passing the software recommended cutoff of 0.511 were considered positive.



479 **Species proteome-wide distribution of Ser/Thr frequency**

480 The protein sequences for *C. albicans* (SC5314), *C. glabrata* (CBS138) and *C. auris* (B11221)  
481 were downloaded from NCBI Assembly database and a custom Python script was used to count  
482 the frequency of serine and threonine residues. The assembly information for the species is in  
483 Table S6 and the script is available in the project GitHub repository.

484 **Structural prediction and visualization for the Hyphal\_reg\_CWP domain**

485 To perform structural predictions using AlphaFold2, we used the Google Colab notebook  
486 ([https://colab.research.google.com/github/deepmind/alphafold/blob/main/notebooks/AlphaFold.i](https://colab.research.google.com/github/deepmind/alphafold/blob/main/notebooks/AlphaFold.ipynb)  
487 [pynb](https://colab.research.google.com/github/deepmind/alphafold/blob/main/notebooks/AlphaFold.ipynb)) authored by the DeepMind team. This is a reduced version of the full AlphaFold version 2  
488 in that it searches a selected portion of the environmental BFD database, and doesn't use  
489 templates. The Amber relaxation step is included, and no other parameters other than the input  
490 sequences are required. Threading-based prediction and identification of structures with similar  
491 folds were performed with the I-TASSER server (Zhang 2008). Model visualization and  
492 annotation were done in PyMol v2.5.2 (Schrödinger, LLC 2021). Secondary structure prediction  
493 for *C. auris* Hil1's central domain was performed using PSIPred (Buchan and Jones 2019).

494 **Dotplot, identification and annotation of sequence variations among *C. auris* Hil genes**

495 To determine the self-similarity and similarity between the eight *C. auris* Hil proteins, we made  
496 dot plots using JDotter (Brodie et al. 2004). The window size and contrast settings were labeled  
497 in the legends for the respective plots. To visualize the length polymorphism among *C. auris*  
498 Hil1 alleles, the multiple sequence alignment was created using Clustal Omega (Sievers et al.  
499 2011) and annotated using Jalview 2 (Waterhouse et al. 2009).

500 To identify polymorphisms in Hil1-Hil4 in diverse *C. auris* strains, we downloaded the  
501 genome sequences for the following strains from NCBI: Clade I - B11205, B13916; Clade II -  
502 B11220, B12043, B13463; Clade III - B11221, B12037, B12631, B17721; Clade IV - B11245,  
503 B12342. The accession numbers can be found in (Muñoz et al. 2021). We used the amino acid  
504 sequences for Hil1-Hil4 from the strain B8441 as query and searched against the nucleotide  
505 sequences using tblastn with the following parameters {-db\_gencode 12 -evalue 1e-150 -  
506 max\_hsps 2}. Orthologs in each strain were manually curated based on the blast hits to either  
507 the PF11765 domain alone or the entire protein query. All Clade II strains are missing Hil1-Hil4.  
508 Several strains in Clade I, III and IV were found to lack one or more Hil proteins (Table 2). But  
509 upon further inspection, it was found that they have significant tblastn hits for part of the query,  
510 e.g., the central domain, and the hits are located at the end of a chromosome, suggesting the

511 possibility of incomplete or misassembled sequences. Further experiments will be needed to  
512 determine if those Hil genes are present or not in those strains.

### 513 **Estimation of dN/dS ratios and testing branch and site models of Hil gene evolution**

514 To test whether there has been relaxed selective constraint or even positive selection acting on  
515 the PF11765 domain during the expansion of the Hil family in *C. auris*, we used the “codeml”  
516 program in PAML (v4.9e) (Yang 2007) to fit and compare a series of “branch models” (Table  
517 S8). The following parameters were used: {seqtype = 1, CodonFreq = 1, model = variable,  
518 NSsites = 0, code = 8, fix\_kappa = 0, kappa = 2, fix\_omega = 0/1, omega = 0.4/1, cleandata =  
519 0}, among which “model”, “fix\_omega” and “omega” vary among the different models. In the  
520 main text, we presented results obtained with “CodonFreq = 1” (F1x4), where the equilibrium  
521 codon frequencies were estimated based on the average nucleotide frequencies regardless of  
522 the codon position. To determine if the results were robust to how codon frequencies were  
523 estimated, we repeated the analysis with “CodonFreq = 0” (Fequal, assuming equal frequency  
524 for all 61 codons) and “CodonFreq = 2” (F3x4, codon frequencies estimated from the nucleotide  
525 frequencies at the three codon positions). The result with “CodonFreq = 0” is nearly identical to  
526 those with the results in the main text. However, the result obtained with “CodonFreq = 2”  
527 identified different branches as having elevated dN/dS ratios (Fig S12). Under this model, the  
528 dS estimates for some branches were >30 substitutions per synonymous site, with a total tree  
529 length - defined as the number of nucleotide substitutions per codon - being 100, compared with  
530 15 and 10 under the F1x4 and the Fequal model, respectively. These unusually large estimates  
531 led us to question the validity of the F3x4 model fits to our dataset. We noticed that in our data  
532 the third codon position is rich in C/T (72%, vs 37% and 55% at the first and second positions)  
533 and has very few A’s (<10%), which may be the cause for the unusual dS estimates.

534 To estimate the pairwise dN/dS ratios between repeats either within or across Hil1 and  
535 Hil2 in *C. auris*, we used the “yn00” program in PAML (v4.9e), which implements the method  
536 described in (Yang and Nielsen 2000). The following parameters were used: {icode = 8,  
537 weighting = 1, common3x4 = 1}. The repeats themselves in the two genes were identified using  
538 XSTREAM as described above and their sequences were manually extracted with the help of  
539 the “getfasta” tool in the BEDtools suite (Quinlan and Hall 2010). In both this and the above  
540 analysis, the coding sequence alignment files were prepared using PAL2NAL.pl (Suyama et al.  
541 2006) with the protein sequence alignment and nucleotide sequence files as input. To test for  
542 differences in the mean of the distribution between the intra- and inter-gene pairwise dN/dS  
543 estimates, we used two-tailed Wilcoxon Rank Sum tests.

## 544 **Chromosomal locations of Hil family genes**

545 Of the 18 species, seven had been assembled to a chromosomal level and are suitable for  
546 determining the chromosomal locations of the Hil family genes (Table S6), i.e., *C. albicans*, *C.*  
547 *dublinsiensis*, *C. glabrata*, *D. hansenii*, *K. lactis*, *N. castellii* and *S. stipitis*. *C. dublinsiensis* was  
548 removed because it is closely related to *C. albicans* and our phylogenetic analysis showed that  
549 most of the Hil family genes in the two species share their duplication history. Similarly, we  
550 removed *N. castellii*, which is redundant with *K. lactis*. We note that while the *C. auris* RefSeq  
551 Assembly (B11221) is still at a scaffold level, a recent study showed that seven of its longest  
552 scaffolds are chromosome-length, thus allowing the mapping of scaffolds to chromosomes  
553 (Muñoz et al. 2021, Supplementary Table 1). We thus included *C. auris* in the downstream  
554 analysis. To determine the chromosomal locations of the Hil homologs in these six species, we  
555 used Rentrez v1.2.3 (Winter 2017) in R to query the NCBI databases with their protein IDs  
556 (scripts available in the project GitHub repository). To calculate the background gene density on  
557 each chromosome, we downloaded the feature tables for the six genomes from NCBI and  
558 calculated the location of each gene as its start coordinate divided by the chromosome length.  
559 To compare the chromosomal locations of Hil family genes to the genome background, we  
560 divided each chromosome into five equal-sized bins based on the distance to the nearest  
561 chromosome end and calculated the proportion of genes residing in each bin either for the Hil  
562 family or for all protein coding genes. To determine if the two distributions differ significantly  
563 from one other, we performed a goodness-of-fit test using either a Log Likelihood Ratio (LLR)  
564 test or a Chi-Square test, as implemented in the XNomial package in R (Engels 2015). The LLR  
565 test is generally preferred and its *P*-value is reported in the results.

## 566 **Acknowledgement**

567 We thank the members of the Gene Regulatory Evolution lab for discussions. Dr. Bin Z. He is  
568 supported by NIH R35GM137831. Lindsey Snyder was supported by the NIH Predoctoral  
569 Training grant T32GM008629. Rachel Smoak is supported by an NSF Graduate Research  
570 Fellowship Program under Grant No. 1546595, with additional support through the NSF Division  
571 of Graduate Education under Grant No. 1633098.

## 572 **Reference**

573 Ai W, Bertram PG, Tsang CK, Chan TF, Zheng XFS. 2002. Regulation of subtelomeric silencing  
574 during stress response. *Mol. Cell* 10:1295–1305.

- 575 Almagro Armenteros JJ, Tsirigos KD, Sønderby CK, Petersen TN, Winther O, Brunak S, von  
576 Heijne G, Nielsen H. 2019. SignalP 5.0 improves signal peptide predictions using deep  
577 neural networks. *Nat. Biotechnol.* 37:420–423.
- 578 Alsteens D, Garcia MC, Lipke PN, Dufrêne YF. 2010. Force-induced formation and propagation  
579 of adhesion nanodomains in living fungal cells. *Proc. Natl. Acad. Sci. U. S. A.*  
580 107:20744–20749.
- 581 Anderson MZ, Wigen LJ, Burrack LS, Berman J. 2015. Real-Time Evolution of a Subtelomeric  
582 Gene Family in *Candida albicans*. *Genetics* 200:907–919.
- 583 Bailey DA, Feldmann PJ, Bovey M, Gow NA, Brown AJ. 1996. The *Candida albicans* HYR1  
584 gene, which is activated in response to hyphal development, belongs to a gene family  
585 encoding yeast cell wall proteins. *J. Bacteriol.* 178:5353–5360.
- 586 Basenko EY, Pulman JA, Shanmugasundram A, Harb OS, Crouch K, Starns D, Warrenfeltz S,  
587 Aurrecochea C, Stoeckert CJ, Kissinger JC, et al. 2018. FungiDB: An Integrated  
588 Bioinformatic Resource for Fungi and Oomycetes. *J. Fungi Basel Switz.* 4:E39.
- 589 Berger SA, Krompass D, Stamatakis A. 2011. Performance, accuracy, and Web server for  
590 evolutionary placement of short sequence reads under maximum likelihood. *Syst. Biol.*  
591 60:291–302.
- 592 Boisramé A, Cornu A, Da Costa G, Richard ML. 2011. Unexpected role for a serine/threonine-  
593 rich domain in the *Candida albicans* Iff protein family. *Eukaryot. Cell* 10:1317–1330.
- 594 Brodie R, Roper RL, Upton C. 2004. JDotter: a Java interface to multiple dotplots generated by  
595 dotter. *Bioinforma. Oxf. Engl.* 20:279–281.
- 596 Buchan DWA, Jones DT. 2019. The PSIPRED Protein Analysis Workbench: 20 years on.  
597 *Nucleic Acids Res.* 47:W402–W407.
- 598 Butler G, Rasmussen MD, Lin MF, Santos MAS, Sakthikumar S, Munro CA, Rheinbay E,  
599 Grabherr M, Forche A, Reedy JL, et al. 2009. Evolution of pathogenicity and sexual  
600 reproduction in eight *Candida* genomes. *Nature* 459:657–662.
- 601 Camacho C, Coulouris G, Avagyan V, Ma N, Papadopoulos J, Bealer K, Madden TL. 2009.  
602 BLAST+: architecture and applications. *BMC Bioinformatics* 10:421.
- 603 Castaño I, Pan S-J, Zupancic M, Hennequin C, Dujon B, Cormack BP. 2005. Telomere length  
604 control and transcriptional regulation of subtelomeric adhesins in *Candida glabrata*. *Mol.*  
605 *Microbiol.* 55:1246–1258.
- 606 CDC. 2019. Antibiotic resistance threats in the United States, 2019. *US Dep. Health Hum. Serv.*  
607 *CDC* [Internet]. Available from: <https://stacks.cdc.gov/view/cdc/82532>
- 608 Chaudhuri R, Ansari FA, Raghunandan MV, Ramachandran S. 2011. FungalRV: adhesin  
609 prediction and immunoinformatics portal for human fungal pathogens. *BMC Genomics*  
610 12:192.

- 611 Chen K, Durand D, Farach-Colton M. 2000. NOTUNG: a program for dating gene duplications  
612 and optimizing gene family trees. *J. Comput. Biol. J. Comput. Mol. Cell Biol.* 7:429–447.
- 613 De Las Peñas A, Pan S-J, Castaño I, Alder J, Cregg R, Cormack BP. 2003. Virulence-related  
614 surface glycoproteins in the yeast pathogen *Candida glabrata* are encoded in  
615 subtelomeric clusters and subject to RAP1- and SIR-dependent transcriptional silencing.  
616 *Genes Dev.* 17:2245–2258.
- 617 Eberlein C, Nielly-Thibault L, Maaroufi H, Dubé AK, Leducq J-B, Charron G, Landry CR. 2017.  
618 The Rapid Evolution of an Ohnolog Contributes to the Ecological Specialization of  
619 Incipient Yeast Species. *Mol. Biol. Evol.* 34:2173–2186.
- 620 Engels B. 2015. XNomial: Exact Goodness-of-Fit Test for Multinomial Data with Fixed  
621 Probabilities. Available from: <https://CRAN.R-project.org/package=XNomial>
- 622 Fernandez-Escamilla A-M, Rousseau F, Schymkowitz J, Serrano L. 2004. Prediction of  
623 sequence-dependent and mutational effects on the aggregation of peptides and  
624 proteins. *Nat. Biotechnol.* 22:1302–1306.
- 625 Frank AT, Ramsook CB, Otoo HN, Tan C, Soybelman G, Rauceo JM, Gaur NK, Klotz SA, Lipke  
626 PN. 2010. Structure and Function of Glycosylated Tandem Repeats from *Candida*  
627 *albicans* Als Adhesins. *Eukaryot. Cell* 9:405–414.
- 628 Frieman MB, McCaffery JM, Cormack BP. 2002. Modular domain structure in the *Candida*  
629 *glabrata* adhesin Epa1p, a beta1,6 glucan-cross-linked cell wall protein. *Mol. Microbiol.*  
630 46:479–492.
- 631 Gabaldón T, Martin T, Marcet-Houben M, Durrens P, Bolotin-Fukuhara M, Lespinet O, Arnaise  
632 S, Boisnard S, Aguilera G, Atanasova R, et al. 2013. Comparative genomics of emerging  
633 pathogens in the *Candida glabrata* clade. *BMC Genomics* 14:623.
- 634 Gabaldón T, Naranjo-Ortiz MA, Marcet-Houben M. 2016. Evolutionary genomics of yeast  
635 pathogens in the Saccharomycotina. *FEMS Yeast Res.* 16.
- 636 de Groot PWJ, Bader O, de Boer AD, Weig M, Chauhan N. 2013. Adhesins in human fungal  
637 pathogens: glue with plenty of stick. *Eukaryot. Cell* 12:470–481.
- 638 Halme A, Bumgarner S, Styles C, Fink GR. 2004. Genetic and Epigenetic Regulation of the FLO  
639 Gene Family Generates Cell-Surface Variation in Yeast. *Cell* 116:405–415.
- 640 Innan H, Kondrashov F. 2010. The evolution of gene duplications: classifying and distinguishing  
641 between models. *Nat. Rev. Genet.* 11:97–108.
- 642 Jenull S, Tscherner M, Kashko N, Shivarathri R, Stoiber A, Chauhan M, Petryshyn A, Chauhan  
643 N, Kuchler K. 2021. Transcriptome Signatures Predict Phenotypic Variations of *Candida*  
644 *auris*. *Front. Cell. Infect. Microbiol.* [Internet] 11. Available from:  
645 <https://www.ncbi.nlm.nih.gov/labs/pmc/articles/PMC8079977/>
- 646 Jumper J, Evans R, Pritzel A, Green T, Figurnov M, Ronneberger O, Tunyasuvunakool K, Bates  
647 R, Židek A, Potapenko A, et al. 2021. Highly accurate protein structure prediction with  
648 AlphaFold. *Nature*:1–11.



- 649 Kean R, Delaney C, Sherry L, Borman A, Johnson EM, Richardson MD, Rautemaa-Richardson  
650 R, Williams C, Ramage G. 2018. Transcriptome Assembly and Profiling of *Candida auris*  
651 Reveals Novel Insights into Biofilm-Mediated Resistance. *mSphere* [Internet] 3.  
652 Available from: <https://msphere.asm.org/content/3/4/e00334-18>
- 653 Kwon YJ, Shin JH, Byun SA, Choi MJ, Won EJ, Lee D, Lee SY, Chun S, Lee JH, Choi HJ, et al.  
654 2019. *Candida auris* Clinical Isolates from South Korea: Identification, Antifungal  
655 Susceptibility, and Genotyping. *J. Clin. Microbiol.* 57:e01624-18.
- 656 Lamoth F, Lockhart SR, Berkow EL, Calandra T. 2018. Changes in the epidemiological  
657 landscape of invasive candidiasis. *J. Antimicrob. Chemother.* 73:i4–i13.
- 658 Linder T, Gustafsson CM. 2008. Molecular phylogenetics of ascomycotal adhesins—A novel  
659 family of putative cell-surface adhesive proteins in fission yeasts. *Fungal Genet. Biol.*  
660 45:485–497.
- 661 Lipke PN. 2018. What We Do Not Know about Fungal Cell Adhesion Molecules. *J. Fungi Basel*  
662 *Switz.* 4.
- 663 Lipke PN, Garcia MC, Alsteens D, Ramsook CB, Klotz SA, Dufrêne YF. 2012. Strengthening  
664 relationships: amyloids create adhesion nanodomains in yeasts. *Trends Microbiol.*  
665 20:59–65.
- 666 Lockhart SR, Etienne KA, Vallabhaneni S, Farooqi J, Chowdhary A, Govender NP, Colombo  
667 AL, Calvo B, Cuomo CA, Desjardins CA, et al. 2017. Simultaneous Emergence of  
668 Multidrug-Resistant *Candida auris* on 3 Continents Confirmed by Whole-Genome  
669 Sequencing and Epidemiological Analyses. *Clin. Infect. Dis. Off. Publ. Infect. Dis. Soc.*  
670 *Am.* 64:134–140.
- 671 Luo G, Ibrahim AS, Spellberg B, Nobile CJ, Mitchell AP, Fu Y. 2010. *Candida albicans* Hyr1p  
672 Confers Resistance to Neutrophil Killing and Is a Potential Vaccine Target. *J. Infect. Dis.*  
673 201:1718–1728.
- 674 Mefford HC, Trask BJ. 2002. The complex structure and dynamic evolution of human  
675 subtelomeres. *Nat. Rev. Genet.* 3:91–102.
- 676 Morel B, Kozlov AM, Stamatakis A, Szöllösi GJ. 2020. GeneRax: A Tool for Species-Tree-  
677 Aware Maximum Likelihood-Based Gene Family Tree Inference under Gene  
678 Duplication, Transfer, and Loss. *Mol. Biol. Evol.* 37:2763–2774.
- 679 Muñoz JF, Gade L, Chow NA, Loparev VN, Juieng P, Berkow EL, Farrer RA, Litvintseva AP,  
680 Cuomo CA. 2018. Genomic insights into multidrug-resistance, mating and virulence in  
681 *Candida auris* and related emerging species. *Nat. Commun.* 9:5346.
- 682 Muñoz JF, Welsh RM, Shea T, Batra D, Gade L, Howard D, Rowe LA, Meis JF, Litvintseva AP,  
683 Cuomo CA. 2021. Clade-specific chromosomal rearrangements and loss of subtelomeric  
684 adhesins in *Candida auris*. *Genetics* [Internet]. Available from:  
685 <https://doi.org/10.1093/genetics/iyab029>



- 686 Newman AM, Cooper JB. 2007. XSTREAM: A practical algorithm for identification and  
687 architecture modeling of tandem repeats in protein sequences. *BMC Bioinformatics*  
688 8:382.
- 689 Otoo HN, Lee KG, Qiu W, Lipke PN. 2008. Candida albicans Als Adhesins Have Conserved  
690 Amyloid-Forming Sequences. *Eukaryot. Cell* 7:776–782.
- 691 Persi E, Wolf YI, Koonin EV. 2016. Positive and strongly relaxed purifying selection drive the  
692 evolution of repeats in proteins. *Nat. Commun.* 7:13570.
- 693 Pierleoni A, Martelli PL, Casadio R. 2008. PredGPI: a GPI-anchor predictor. *BMC Bioinformatics*  
694 9:392.
- 695 Potter SC, Luciani A, Eddy SR, Park Y, Lopez R, Finn RD. 2018. HMMER web server: 2018  
696 update. *Nucleic Acids Res.* 46:W200–W204.
- 697 Qian W, Zhang JG. 2014. Genomic evidence for adaptation by gene duplication. *Genome*  
698 *Res.:*gr.172098.114.
- 699 Quinlan AR, Hall IM. 2010. BEDTools: a flexible suite of utilities for comparing genomic  
700 features. *Bioinformatics* 26:841–842.
- 701 R Core Team. R: A Language and Environment for Statistical Computing. Vienna, Austria: R  
702 Foundation for Statistical Computing Available from: <https://www.R-project.org>
- 703 Ramsook CB, Tan C, Garcia MC, Fung R, Soybelman G, Henry R, Litewka A, O’Meally S, Otoo  
704 HN, Khalaf RA, et al. 2010. Yeast cell adhesion molecules have functional amyloid-  
705 forming sequences. *Eukaryot. Cell* 9:393–404.
- 706 Rauceo JM, De Armond R, Otoo H, Kahn PC, Klotz SA, Gaur NK, Lipke PN. 2006. Threonine-  
707 rich repeats increase fibronectin binding in the Candida albicans adhesin Als5p.  
708 *Eukaryot. Cell* 5:1664–1673.
- 709 Reithofer V, Fernández-Pereira J, Alvarado M, de Groot P, Essen L-O. 2021. A novel class of  
710 Candida glabrata cell wall proteins with  $\beta$ -helix fold mediates adhesion in clinical  
711 isolates. *PLoS Pathog.* 17:e1009980.
- 712 Rice P, Longden I, Bleasby A. 2000. EMBOSS: the European Molecular Biology Open Software  
713 Suite. *Trends Genet. TIG* 16:276–277.
- 714 Richard ML, Plaine A. 2007. Comprehensive Analysis of Glycosylphosphatidylinositol-Anchored  
715 Proteins in Candida albicans. *Eukaryot. Cell* 6:119–133.
- 716 Rosiana S, Zhang L, Kim GH, Revtovich AV, Uthayakumar D, Sukumaran A, Geddes-McAlister  
717 J, Kirienko NV, Shapiro RS. 2021. Comprehensive genetic analysis of adhesin proteins  
718 and their role in virulence of Candida albicans. *Genetics* [Internet]. Available from:  
719 <https://doi.org/10.1093/genetics/iyab003>
- 720 RStudio Team. 2021. RStudio: Integrated Development Environment for R. Boston, MA:  
721 RStudio, PBC Available from: <http://www.rstudio.com/>

- 722 Schrödinger, LLC. 2021. The PyMOL Molecular Graphics System, Version 2.5.2.
- 723 Sequeira S, Kavanaugh D, MacKenzie DA, Šuligoj T, Walpole S, Leclaire C, Gunning AP,  
724 Latousakis D, Willats WGT, Angulo J, et al. 2018. Structural basis for the role of serine-  
725 rich repeat proteins from *Lactobacillus reuteri* in gut microbe–host interactions. *Proc.*  
726 *Natl. Acad. Sci.* 115:E2706–E2715.
- 727 Shen X-X, Opulente DA, Kominek J, Zhou X, Steenwyk JL, Buh KV, Haase MAB, Wisecaver  
728 JH, Wang M, Doering DT, et al. 2018. Tempo and Mode of Genome Evolution in the  
729 Budding Yeast Subphylum. *Cell* [Internet]. Available from:  
730 <http://www.sciencedirect.com/science/article/pii/S0092867418313321>
- 731 Sievers F, Wilm A, Dineen D, Gibson TJ, Karplus K, Li W, Lopez R, McWilliam H, Remmert M,  
732 Söding J, et al. 2011. Fast, scalable generation of high-quality protein multiple sequence  
733 alignments using Clustal Omega. *Mol. Syst. Biol.* 7:539.
- 734 Singh S, Uppuluri P, Mamouei Z, Alqarihi A, Elhassan H, French S, Lockhart SR, Chiller T, Jr  
735 JEE, Ibrahim AS. 2019. The NDV-3A vaccine protects mice from multidrug resistant  
736 *Candida auris* infection. *PLOS Pathog.* 15:e1007460.
- 737 Snoek T, Voordeckers K, Verstrepen KJ. 2014. Subtelomeric Regions Promote Evolutionary  
738 Innovation of Gene Families in Yeast. In: Louis EJ, Becker MM, editors. Subtelomeres.  
739 Berlin, Heidelberg: Springer. p. 39–70. Available from: [https://doi.org/10.1007/978-3-](https://doi.org/10.1007/978-3-642-41566-1_3)  
740 [642-41566-1\\_3](https://doi.org/10.1007/978-3-642-41566-1_3)
- 741 Srivastava V, Singla RK, Dubey AK. 2018. Emerging virulence, drug resistance and future anti-  
742 fungal drugs for *Candida* pathogens. *Curr. Top. Med. Chem.*
- 743 Stamatakis A. 2014. RAxML version 8: a tool for phylogenetic analysis and post-analysis of  
744 large phylogenies. *Bioinformatics* 30:1312–1313.
- 745 Suyama M, Torrents D, Bork P. 2006. PAL2NAL: robust conversion of protein sequence  
746 alignments into the corresponding codon alignments. *Nucleic Acids Res.* 34:W609-612.
- 747 Teunissen AW, Steensma HY. 1995. Review: the dominant flocculation genes of  
748 *Saccharomyces cerevisiae* constitute a new subtelomeric gene family. *Yeast Chichester*  
749 *Engl.* 11:1001–1013.
- 750 Uppuluri P, Lin L, Alqarihi A, Luo G, Youssef EG, Alkhazraji S, Yount NY, Ibrahim BA, Bolaris  
751 MA, Edwards JE, et al. 2018. The Hyr1 protein from the fungus *Candida albicans* is a  
752 cross kingdom immunotherapeutic target for *Acinetobacter* bacterial infection. *PLoS*  
753 *Pathog.* [Internet] 14. Available from:  
754 <https://www.ncbi.nlm.nih.gov/pmc/articles/PMC5963808/>
- 755 Verstrepen KJ, Jansen A, Lewitter F, Fink GR. 2005. Intragenic tandem repeats generate  
756 functional variability. *Nat. Genet.* 37:986–990.
- 757 Verstrepen KJ, Reynolds TB, Fink GR. 2004. Origins of variation in the fungal cell surface. *Nat.*  
758 *Rev. Microbiol.* 2:533–540.

- 759 Wang L-G, Lam TT-Y, Xu S, Dai Z, Zhou L, Feng T, Guo P, Dunn CW, Jones BR, Bradley T, et  
760 al. 2020. Treeio: An R Package for Phylogenetic Tree Input and Output with Richly  
761 Annotated and Associated Data. *Mol. Biol. Evol.* 37:599–603.
- 762 Waterhouse A, Bertoni M, Bienert S, Studer G, Tauriello G, Gumienny R, Heer FT, de Beer  
763 TAP, Rempfer C, Bordoli L, et al. 2018. SWISS-MODEL: homology modelling of protein  
764 structures and complexes. *Nucleic Acids Res.* 46:W296–W303.
- 765 Waterhouse AM, Procter JB, Martin DMA, Clamp M, Barton GJ. 2009. Jalview Version 2--a  
766 multiple sequence alignment editor and analysis workbench. *Bioinforma. Oxf. Engl.*  
767 25:1189–1191.
- 768 Welsh RM, Sexton DJ, Forsberg K, Vallabhaneni S, Litvintseva A. 2019. Insights into the  
769 Unique Nature of the East Asian Clade of the Emerging Pathogenic Yeast *Candida*  
770 *auris*. *J. Clin. Microbiol.* 57:e00007-19.
- 771 Wilkins M, Zhang N, Schmid J. 2018. Biological Roles of Protein-Coding Tandem Repeats in the  
772 Yeast *Candida Albicans*. *J. Fungi* 4:78.
- 773 Willaert R. 2018. Adhesins of Yeasts: Protein Structure and Interactions. *J. Fungi* 4:119.
- 774 Winter DJ. 2017. rentrez: an R package for the NCBI eUtils API. *R J.* 9:520–526.
- 775 Xu Z, Green B, Benoit N, Sobel JD, Schatz MC, Wheelan S, Cormack BP. 2021. Cell wall  
776 protein variation, break-induced replication, and subtelomere dynamics in *Candida*  
777 *glabrata*. *Mol. Microbiol.*
- 778 Yang Z. 1998. Likelihood ratio tests for detecting positive selection and application to primate  
779 lysozyme evolution. *Mol. Biol. Evol.* 15:568–573.
- 780 Yang Z. 2007. PAML 4: Phylogenetic Analysis by Maximum Likelihood. *Mol. Biol. Evol.*  
781 24:1586–1591.
- 782 Yang Z, Nielsen R. 2000. Estimating synonymous and nonsynonymous substitution rates under  
783 realistic evolutionary models. *Mol. Biol. Evol.* 17:32–43.
- 784 Yu G. 2020. Using ggtree to Visualize Data on Tree-Like Structures. *Curr. Protoc. Bioinforma.*  
785 69:e96.
- 786 Zhang J. 2003. Evolution by gene duplication: an update. *Trends Ecol. Evol.* 18:292–298.
- 787 Zhang J. 2006. Parallel adaptive origins of digestive RNases in Asian and African leaf monkeys.  
788 *Nat. Genet.* 38:819–823.
- 789 Zhang Y. 2008. I-TASSER server for protein 3D structure prediction. *BMC Bioinformatics* 9:40.
- 790 Zhen Y, Aardema ML, Medina EM, Schumer M, Andolfatto P. 2012. Parallel Molecular Evolution  
791 in an Herbivore Community. *Science* 337:1634–1637.
- 792  
793

794 Table 1. Top structural templates for *C. auris* Hil PF11765 domains

PDB Hit	Species	Organism	Protein / Domain	Function
5ke1A	<i>Shigella flexneri</i>	gram-negative bacterium	IcsA/VirG passenger-domain	adhesin and actin-polymerizing factor
5nxkA	<i>Limosilactobacillus reuteri</i>	gram-positive bacterium	Serine-Rich Repeat Protein binding domain	adhesin
3ogzA	<i>Leishmania major</i>	trypanosomes	UDP-sugar pyrophosphorylase	sugar pyrophosphorylase with broad substrate specificity
5ny0A	<i>Limosilactobacillus reuteri</i>	gram-positive bacterium	Serine-Rich Repeat Protein binding domain	adhesin
4kh3A	<i>Escherichia coli</i>	gram-negative bacterium	bacterial self-associating protein	self-association and cell aggregation
6n2bA	<i>Caldicellulosiruptor kristjanssonii</i>	gram-positive bacterium	Tapirin C-terminal domain	cellulose-binding, adhesion

795  
796

797 Table 2. Intraspecific variation in tandem repeat copy number in *C. auris* Hil1-4

Clade / Strain	Tandem repeat: copy number (repeat period)			
	Hil1	Hil2	Hil3	Hil4
Clade I				
B8441	46 (44)	21 (44)	16 (51)	15 (47)
B11205	46 (44)	21 (44)	16 (51)	15 (47)
B13916	46 (44)	21 (44)	16 (51)	15 (47)
Clade III				
B11221	48 (44)	20* (44)	16 (51)	NA
B17721	48 (44)	21 (44)	16 (51)	14 (48)
B12037	48 (44)	NA	16 (51)	14 (48)
B12631	NA	NA	16 (51)	14 (48)
Clade IV				
B12342	48 (43)	15 (44)	11 (51)	15 (47)
B11245	NA	15 (44)	11 (51)	15 (47)

798 \* deletion of 16 aa, not a full repeat

799 NA: homolog not identified in the strain's genome by tblastn

800

801 Table 3. Likelihood ratio tests for different dN/dS ratios

Alternative Hypothesis	Null Hypothesis	Assumption Made	$2\Delta\ell$	Models Compared
a. $(\omega_1=\omega_2) \neq \omega_0$	$(\omega_1 = \omega_2) = \omega_0$	$\omega_1 = \omega_2$	24.74***	A and D
b. $\omega_1 \neq \omega_0$	$\omega_1 = \omega_0$	$\omega_2 = \omega_0$	17.92***	A and B
c. $\omega_2 \neq \omega_0$	$\omega_2 = \omega_0$	$\omega_1 = \omega_0$	7.18**	A and C
d. $(\omega_1=\omega_2) > 1$	$(\omega_1 = \omega_2) \leq 1$	$\omega_1 = \omega_2$	4.2*	D and G
e. $\omega_1 > 1$	$\omega_1 \leq 1$	$\omega_2 = \omega_0$	2.68	B and E
f. $\omega_2 > 1$	$\omega_2 \leq 1$	$\omega_1 = \omega_0$	1.74	C and F
g. $\omega_3 \neq \omega_0$	$\omega_3 = \omega_0$	$(\omega_1 = \omega_2)$ free	47.14***	D and H

802 Designations for the different  $\omega$  values can be found in Fig 5A;  $2\Delta\ell = 2x$  log likelihood difference between the two  
803 models being compared, where the models and their parameter estimates can be found in Table S8. Tests significant  
804 at 0.001, 0.01 and 0.05 levels are labeled with three, two and one asterisk(s), with  $P$ -values based on a  $\chi^2$  distribution  
805 with 1 degree of freedom.



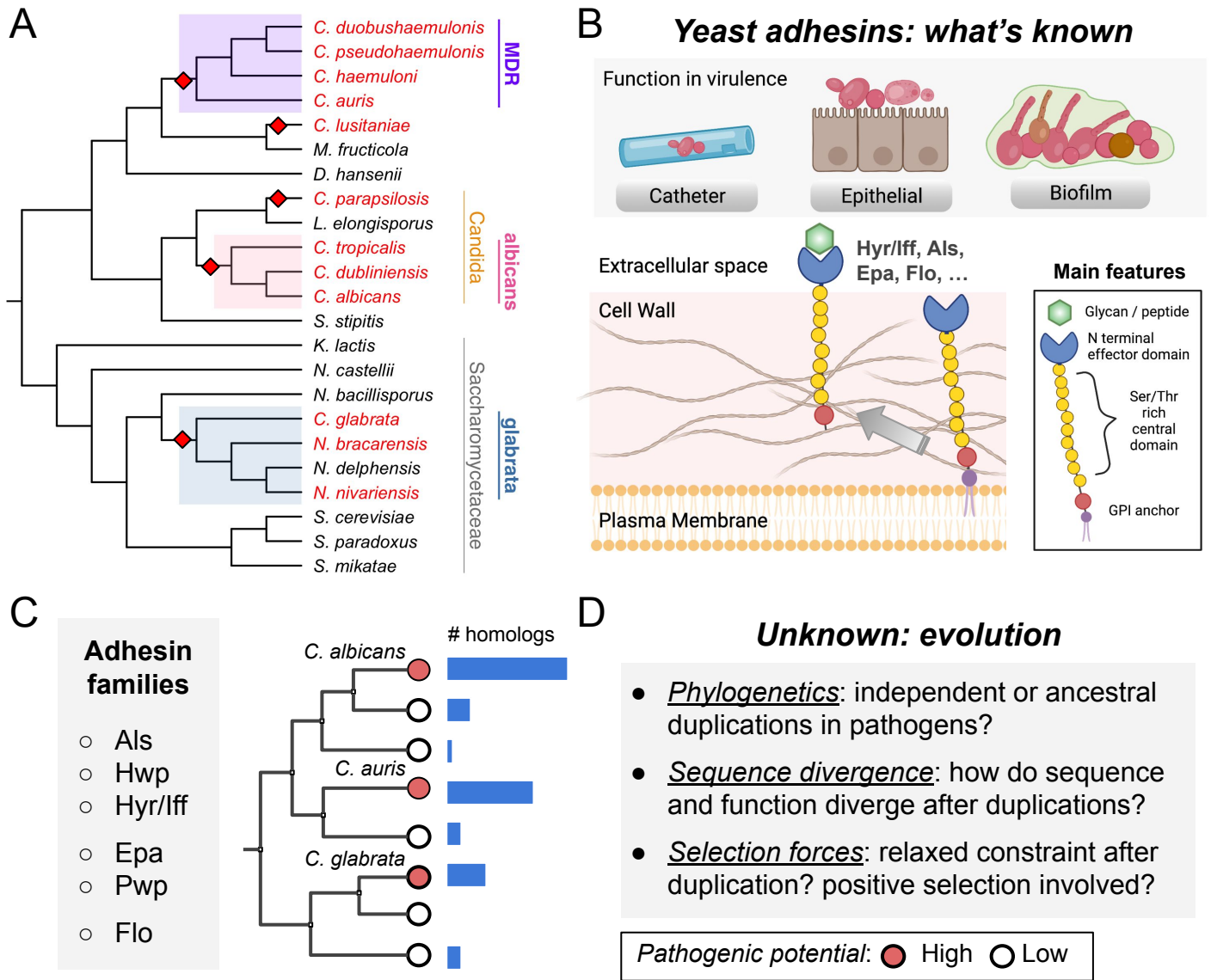


**Figure 1. Multiple origins of yeast pathogens and evolution of yeast adhesin families.** (A) Species phylogeny suggesting multiple origins of yeast pathogens. Species known to be pathogenic are in red and species never or rarely identified as pathogens are in black. Diamonds represent potential origination of pathogenesis, which are enriched in the highlighted *glabrata*, *albicans* and multidrug-resistant (MDR) clades. (B) As cell-wall proteins, yeast adhesins are initially inserted into the plasma membrane; most are then cleaved at the C-terminal GPI-anchor, the remnant of which allow them to be covalently linked to the  $\beta$ -1,6-glucan in the cell wall. The central stalk (yellow circles) is glycosylated at the Ser/Thr residues, which enables it to adopt a rigid, rod-like shape that helps to push out the N-terminal effector domain. The latter binds glycan or peptide substrates and mediates adhesion to other yeasts, host epithelium or inanimate surfaces. Drawing partly based on (Verstrepen and Klis 2006) and created with BioRender.com (C) Left: examples of known yeast adhesin families in *C. albicans* (first three), *C. glabrata* (middle two) and *S. cerevisiae* (last). Right: a species tree showing the larger size of an adhesin family in the pathogenic species. (D) The evolutionary questions to be addressed in this study. Full species names in (A): *Candida duobushaemulonius*, *Candida pseudohaemulonius*, *Candida haemulonii*, *Candida auris*, *Clavispora lusitanae*, *Metschnikowia fructicola*, *Debaryomyces hansenii*, *Candida parapsilosis*, *Lodderomyces elongisporus*, *Candida tropicalis*, *Candida dubliniensis*, *Candida albicans*, *Scheffersomyces stipitis*, *Kluyveromyces lactis*, *Naumovozyma castellii*, *Nakaseomyces bacillisporus*, *Candida glabrata*, *Nakaseomyces braccarensis*, *Nakaseomyces delphensis*, *Nakaseomyces nivariensis*, *Saccharomyces cerevisiae*, *Saccharomyces paradoxus*, *Saccharomyces mikatae*

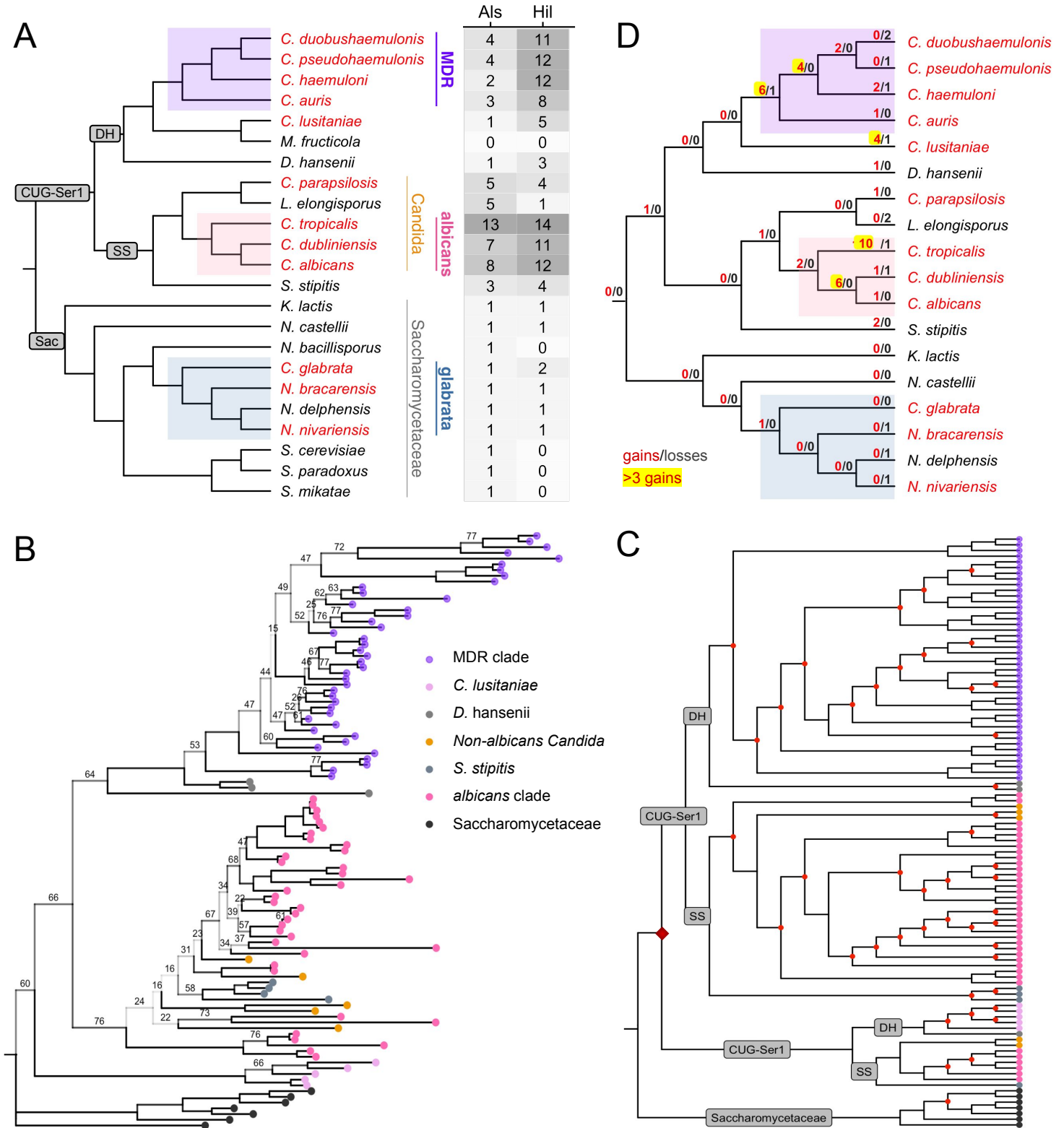


**Figure 2. Parallel expansion of the Hil family in independently derived pathogenic *Candida* lineages.**  
Legend on next page

**Figure 2. Parallel expansion of the Hil family in independently derived pathogenic *Candida* lineages.** (A) Same species tree as in Fig 1A, with gray labels in the inner nodes corresponding to those in panel C. The size of two adhesin families found in both *C. albicans* and *C. auris* are shown. (B) Maximum likelihood tree based on the binding domain of the Hil family is shown as a phylogram, rooted on the Saccharomycetaceae group. Branches with lower rapid bootstrap support by RAxML are shown as semi-transparent lines; bootstrap values lower than 80% are labeled. (C) Reconciled gene tree shown in cladogram. Gray labels highlight the important clades, including the outgroup of Saccharomycetaceae, the two CUG-Ser1 groups following an ancient duplication (red diamond) and within each branch, the *Candida* and *Clavispora* sequences labeled by their respective outgroups, *D. hansenii* (DH) and *S. stipitis* (SS). Inferred duplication events are labeled with a red circle, except for the CUG-Ser1 duplication mentioned above. (D) Species tree showing the inferred number of duplications (red) and losses (gray). Three or more duplications are highlighted in yellow. Species with zero Hil family homologs are not shown.

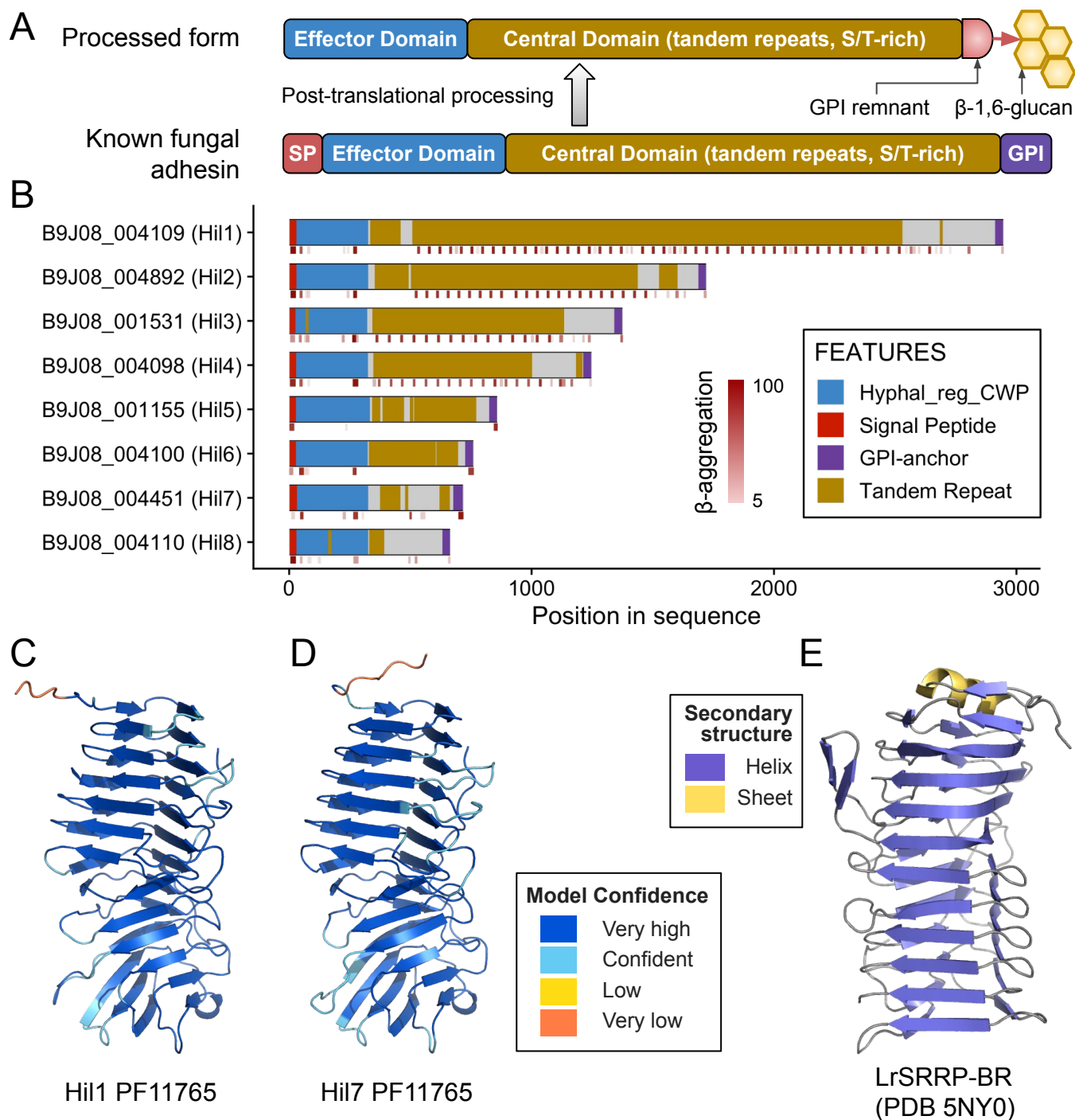


**Figure 3. Domain architecture and predicted effector domain structures support *C. auris* Hil proteins as adhesins.** (A) Diagram depicting a typical yeast adhesin's domain organization, before and after the post-translational processing. Adapted from (de Groot et al. 2013). (B) Domain features of the eight Hil proteins in *C. auris* (strain B8441). Gene IDs and names designated in this study are labeled on the left. The short stripes below each diagram are the TANGO predicted  $\beta$ -aggregation prone sequences, with the intensity of the color corresponding to the score of the prediction. (C) and (D) are AlphaFold2 predicted structures of the PF11765 domains from Hil1 and Hil7. Colors represent the local confidence score (pLDDT). (E) Experimentally determined structure of the Binding Region of the Serine-Rich-Repeat-Protein (SRRP-BR) from *L. reuteri*. Colors represent the secondary structure assignments.



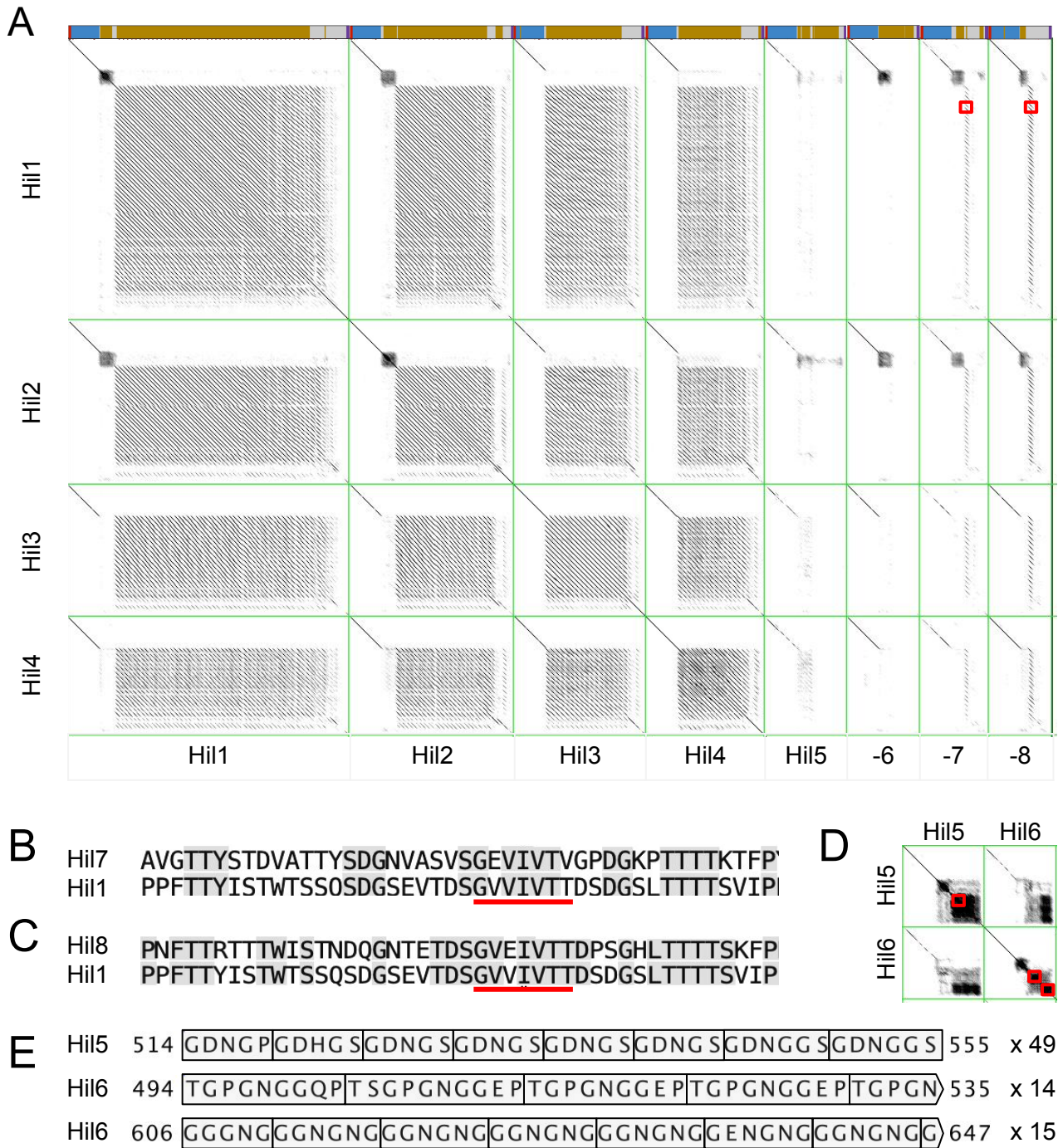


**Figure 4. Dotplot shows the tandem repeat structure within and similarity between *C. auris* Hil proteins.** (A) Dotplot (JDotter, Brodie et al 2004) with a sliding window of 50 aa and Grey Map set to 60-245 (min-max). Hil1-4 are compared to all eight Hil proteins including themselves. A schematic was included for each protein on the top (colors same as in Fig 3). The regions highlighted by the red boxes in row 1 are shown as sequence alignment in (B) and (C) to demonstrate the presence of a single copy of the repeat in Hil7, 8. Shadings indicate sequence similarity and the red underlines highlight the predicted  $\beta$ -aggregation prone sequence. (D) Dotplot between Hil5 and Hil6 with the same settings as in (A), showing the low complexity repeats unique to these two. Regions within the three red boxes are shown in (E), with limits shown on both ends of the sequences. The rectangles delineate individual repeats, with the copy numbers shown to the right. The last copy, when truncated, is indicated by a pointed shape.

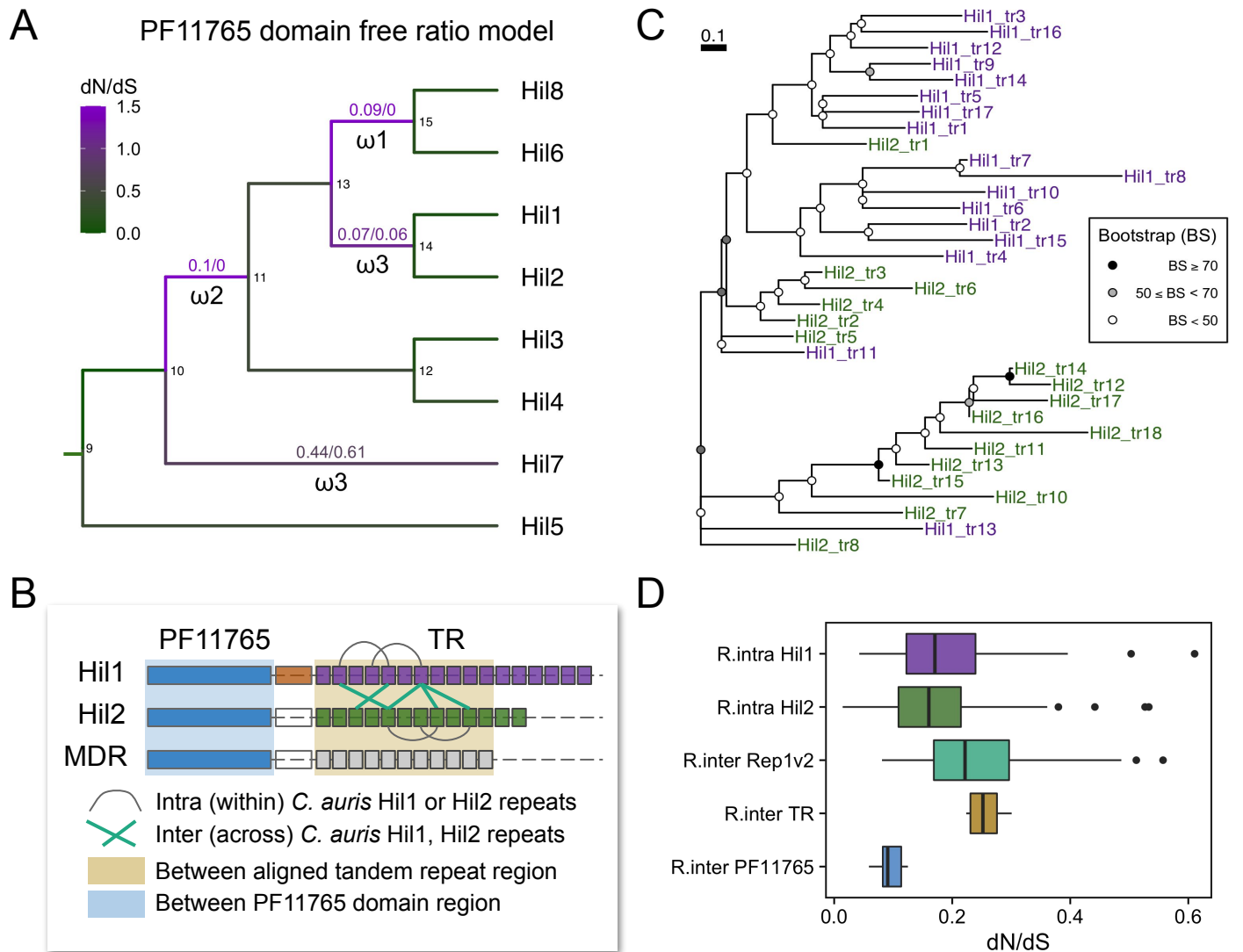


**Figure 5. Selective forces on the PF11765 domain in the *C. auris* Hil genes and the expansion of the tandem repeats within Hil1 and Hil2.** (A) Phylogenetic tree for Hil1-Hil8 from *C. auris* is based on the PF11765 sequence and shown as a cladogram. Branch colors are based on the estimated dN/dS values. For those with dN/dS > 0.5, the estimates of dN and dS are shown above the branch. The  $\omega_1/2/3$  below the branches are foreground values used for the branch tests in Table 3. (B) Schematic for the comparisons in D: pairwise dN/dS ratios are estimated between individual 44aa repeats within Hil1 or Hil2 (R.intra Hil1/2, horizontal evolution) or across the two proteins (R.inter Rep1vs2, vertical evolution). An alternative to the “vertical evolution” estimate assumes an aligned portion of the tandem repeat domain is orthologous and pairwise estimates of dN/dS were obtained for *C. auris* Hil1, Hil2 and closely related MDR clade homologs (R.inter TR). For comparison, pairwise dN/dS ratios were also estimated for the PF11765 domain (R.inter PF11765). The orange box between the PF11765 and TR domains indicates a Serine-rich repeat region only present in Hil1. (C) Maximum likelihood tree for the first 17 repeats from Hil1 and Hil2 suggests most of the repeats likely originated after gene duplication. Branch length is in the unit of substitutions per codon. Repeats from Hil1 are in purple and those from Hil2 are in green. White, gray or black circles on the ancestral nodes indicate bootstrap support levels. (D) Pairwise dN/dS ratios estimated using the YN00 program in PAML are shown as boxplots, where the box shows the interquartile range (IQR), the upper and lower whiskers extend to the largest and smallest values no further than 1.5 x IQR, the middle line shows the median and dots show outliers beyond the 1.5 x IQR.



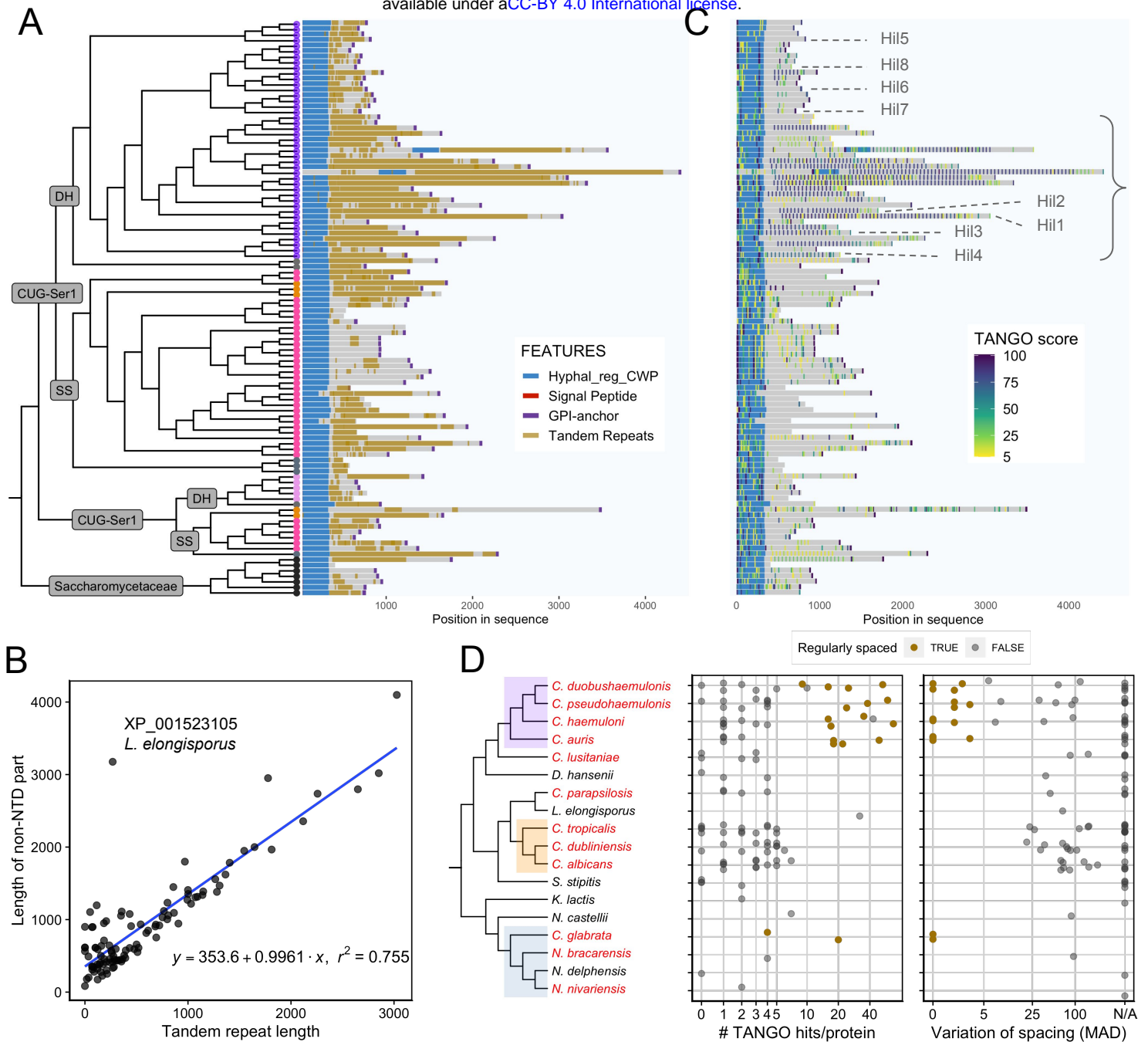


**Figure 6. Divergence in the yeast Hil family in length and central domain features.** (A) Domain architecture plot showing that the majority of the homologs have a signal peptide and a GPI-anchor at the two termini, with the PF11765 domain at the N-terminus followed by a central domain that is highly repetitive. (B) x-y plot showing length of the non-PF11765 (NTD) portion of a Hil family protein as a function of the length of its tandem repeat sequences. The linear regression line is shown in blue, with parameters and  $r^2$  values below. An outlier to the trend is labeled. (C) Distribution of TANGO predicted  $\beta$ -aggregation sequences. The median per-residue probability is used as the score for each sequence and is shown in a color gradient. A group of MDR clade sequences are labeled by a curly bracket. These sequences uniquely harbor a large number of regularly spaced TANGO hits. The eight *C. auris* Hil genes are labeled. (D) The left panel shows the species tree. The middle panel plots the number of strong TANGO hits (score  $\geq 30$ ) per sequence, grouped by the species, and the right plot shows the variance in their inter-TANGO-hit spacing for the same proteins (MAD = median absolute deviation). Proteins with more than three strong TANGO hits and a MAD of the spacing less than 5 residues are labeled as “regularly spaced” and shown in gold color.

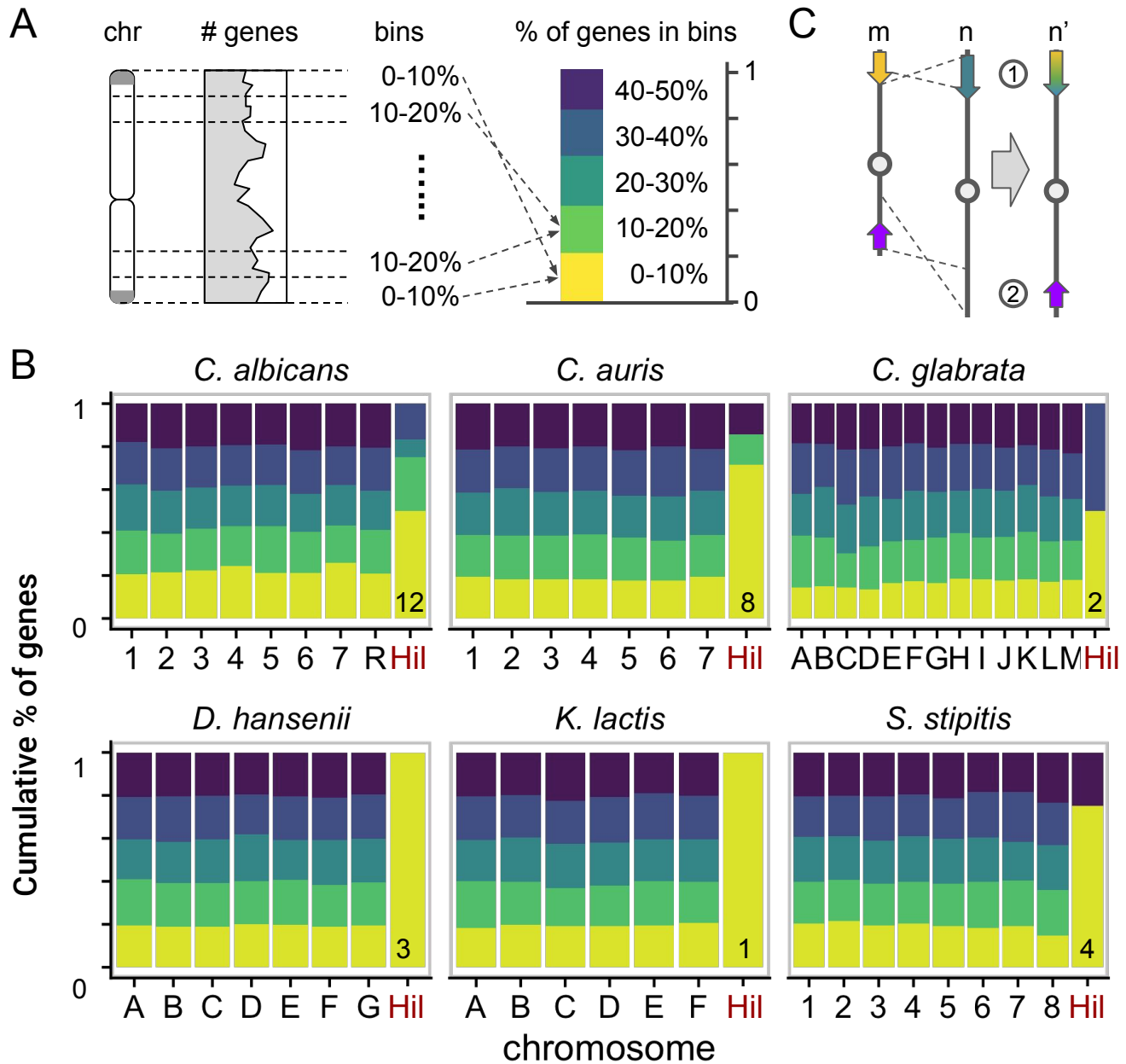
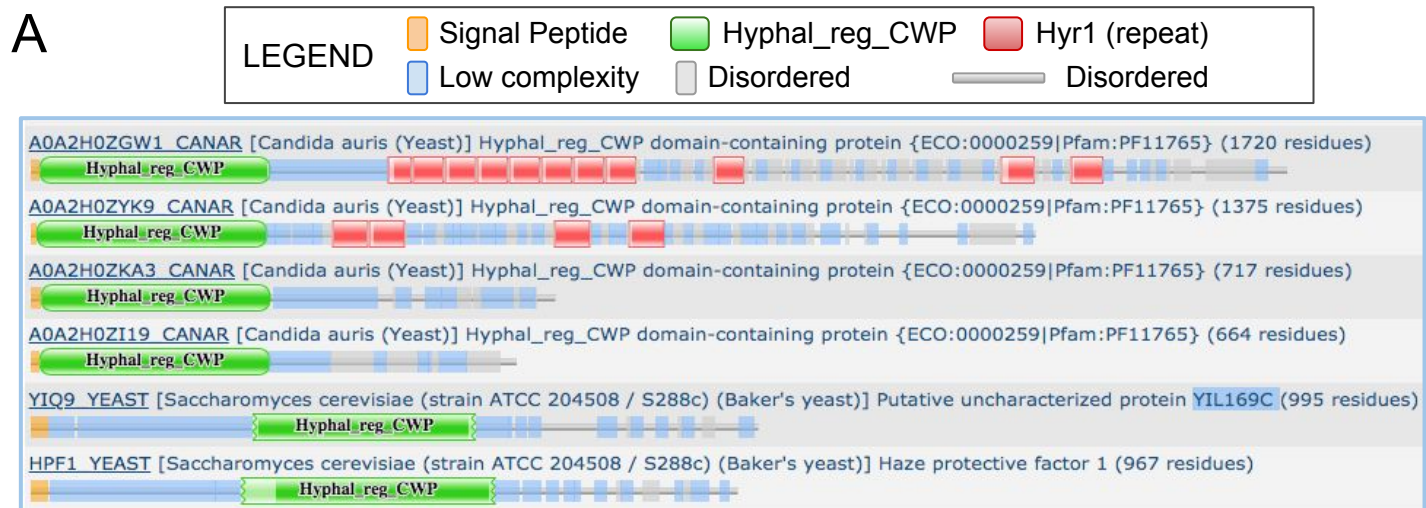


**Figure 7. Hil homologs are preferentially located towards the chromosome ends.** (A) Schematic of the analysis: each chromosome (chr) is folded and divided into five equal-length “bins” that are ordered by their distance to the nearest telomere (gray). The cumulative bar graph on the right summarizes the distribution of genes along the chromosome. (B) This method is applied to six species with a chromosomal level assembly. The Hil homologs in each species are plotted in their own group with the family size labeled at the bottom. A goodness-of-fit test comparing the distribution of the Hil genes to the genome background yielded a  $P$ -value of  $3.6 \times 10^{-6}$ . (C) Ectopic recombination between subteleres could facilitate (1) creation of a new family member by recombination between two existing members and (2) duplication of a subteleric gene onto the equivalent region on a different chromosome.

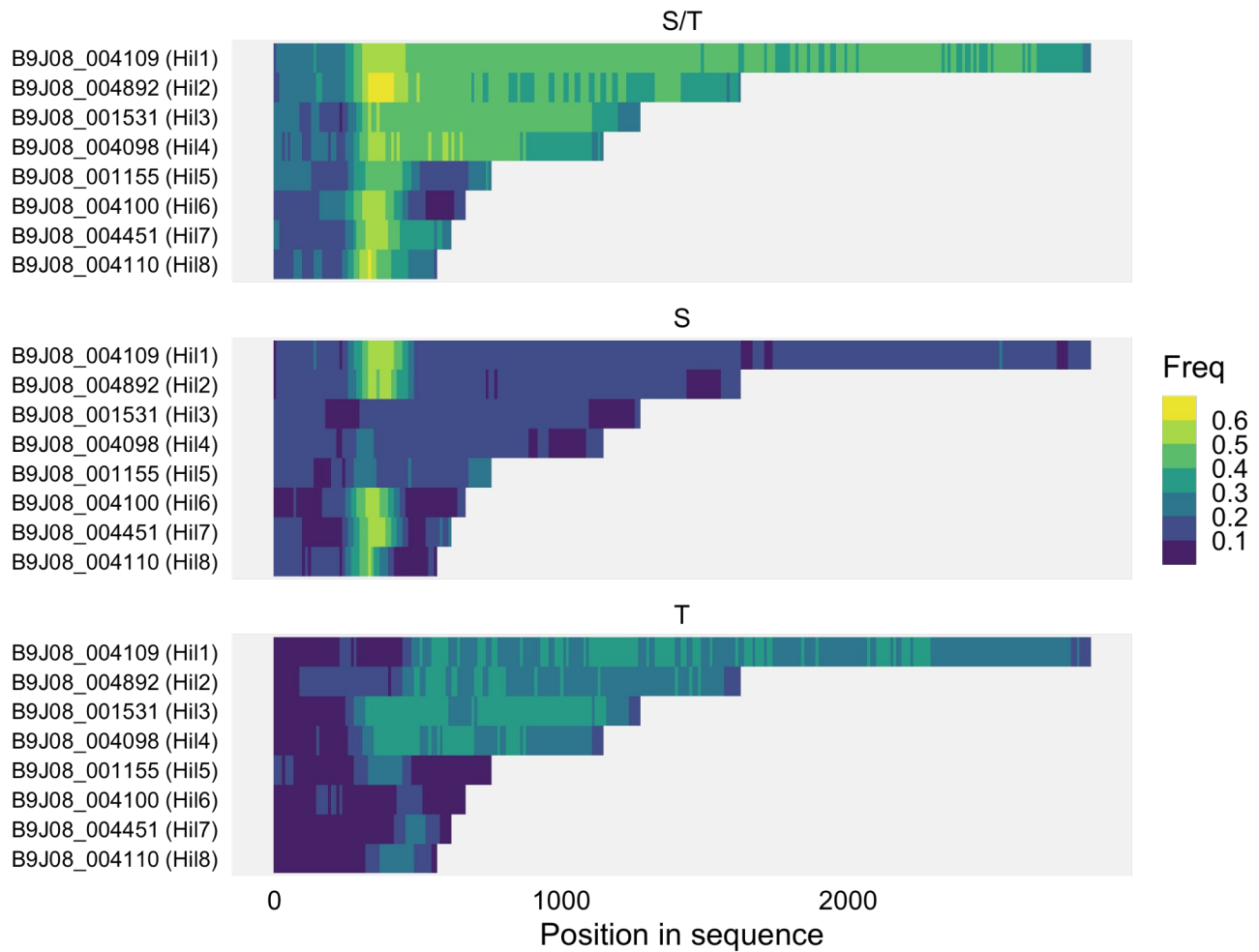


**B**

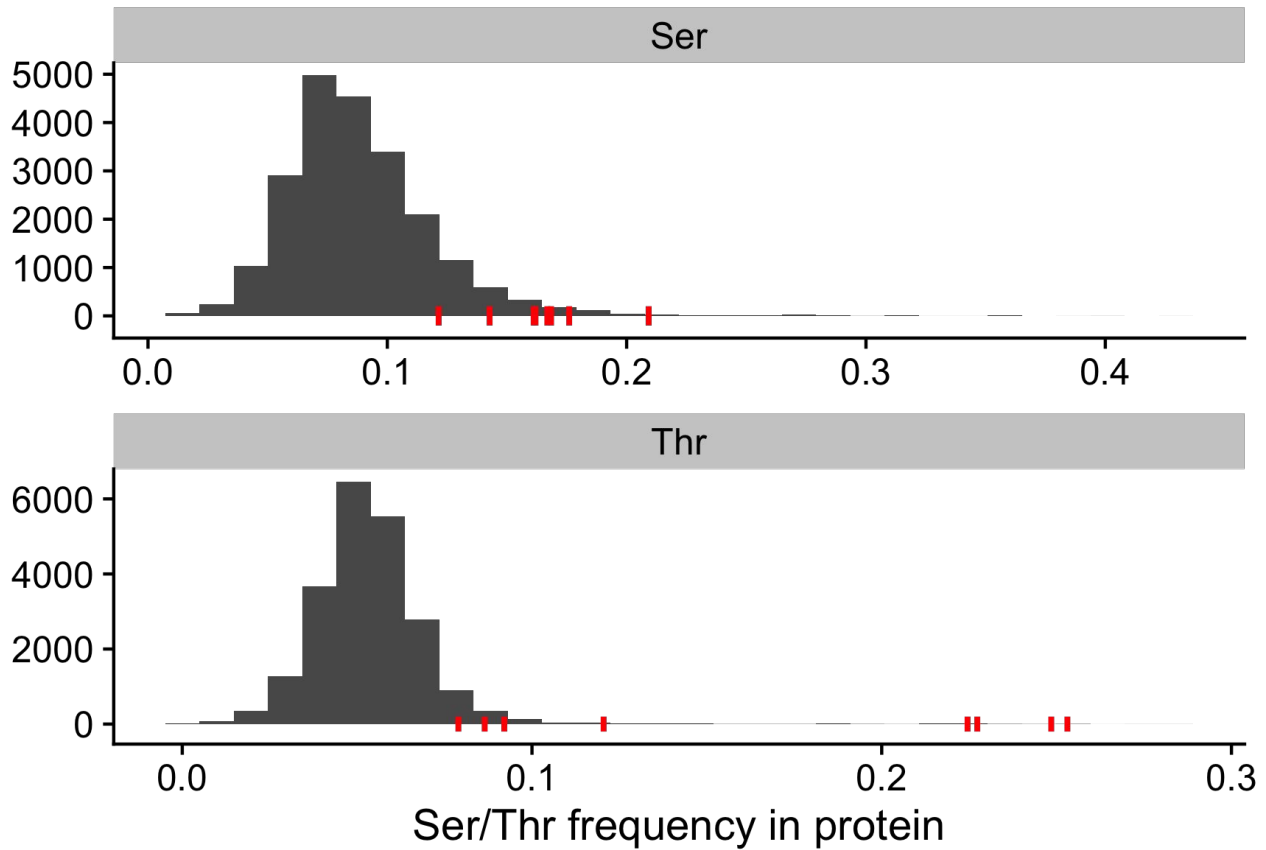
	Description	Max Score	Total Score	Query Cover	E value	Per. Ident	Accession
<input checked="" type="checkbox"/>	<a href="#">CAGL0I07293g_XP_447567.2_Hyphal_reg_CWP</a>	83.2	83.2	91%	4e-22	28.12%	Query_13989
<input checked="" type="checkbox"/>	<a href="#">CAGL0E06600g_XP_445977.1_Hyphal_reg_CWP</a>	76.6	93.2	98%	8e-20	28.31%	Query_13986
<input checked="" type="checkbox"/>	<a href="#">YOL155C_HPFI</a>	42.0	58.5	56%	3e-08	27.66%	Query_13988
<input checked="" type="checkbox"/>	<a href="#">YIL169C_CSS1_Hyp_reg_CWP</a>	39.3	39.3	76%	2e-07	23.78%	Query_13987

**Supplementary figure 1. Two *S. cerevisiae* proteins with the PF11765 domain have different architecture and are more divergent from *C. auris* Hil proteins than Hil homologs from the equally distant *C. glabrata*.** (A) Comparing the domain architectures of the two *S. cerevisiae* proteins with the PF11765 (Hyphal\_reg\_CWP) domain to the Hil homologs from *C. auris*. Notice the *S. cerevisiae* proteins are distinct in that their PF11765 domain is in the middle rather than the N-terminus of the protein. (B) BLASTP comparison with *C. auris* Hil1's PF11765 domain as query and the two *C. glabrata* and two *S. cerevisiae* proteins as subjects. *C. glabrata* is in the same family as *S. cerevisiae* and equally distantly related to *C. auris*. Notice the much lower query coverage and less significant E-values for the *S. cerevisiae* sequences.

## Ser/Thr frequency in 100 aa sliding windows



**Supplementary figure 2. Ser/Thr frequency in the *C. auris* Hil family.** The Ser+Thr or the individual amino acid frequencies were calculated in 100 aa sliding windows with a step size of 10 aa and plotted as a heatmap.

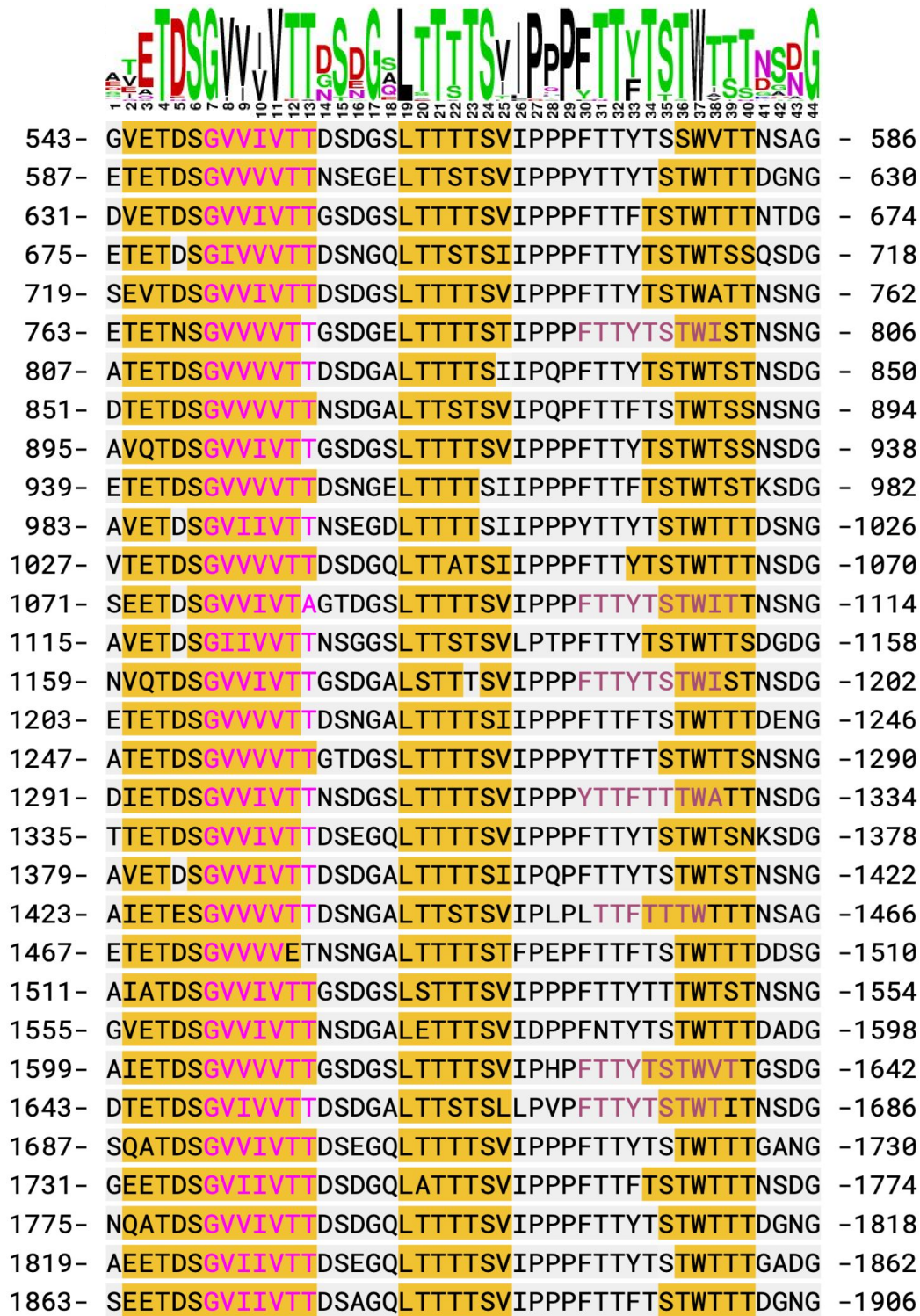


**Supplementary figure 3. Comparing the Ser/Thr frequencies in *C. auris* Hil family members with all protein-coding genes in *C. auris*.** B8441 strain genome is used for this analysis. The frequency of Ser or Thr residues as a percent of the entire protein is plotted as a histogram for all protein-coding genes. Red ticks indicate the eight Hil genes.

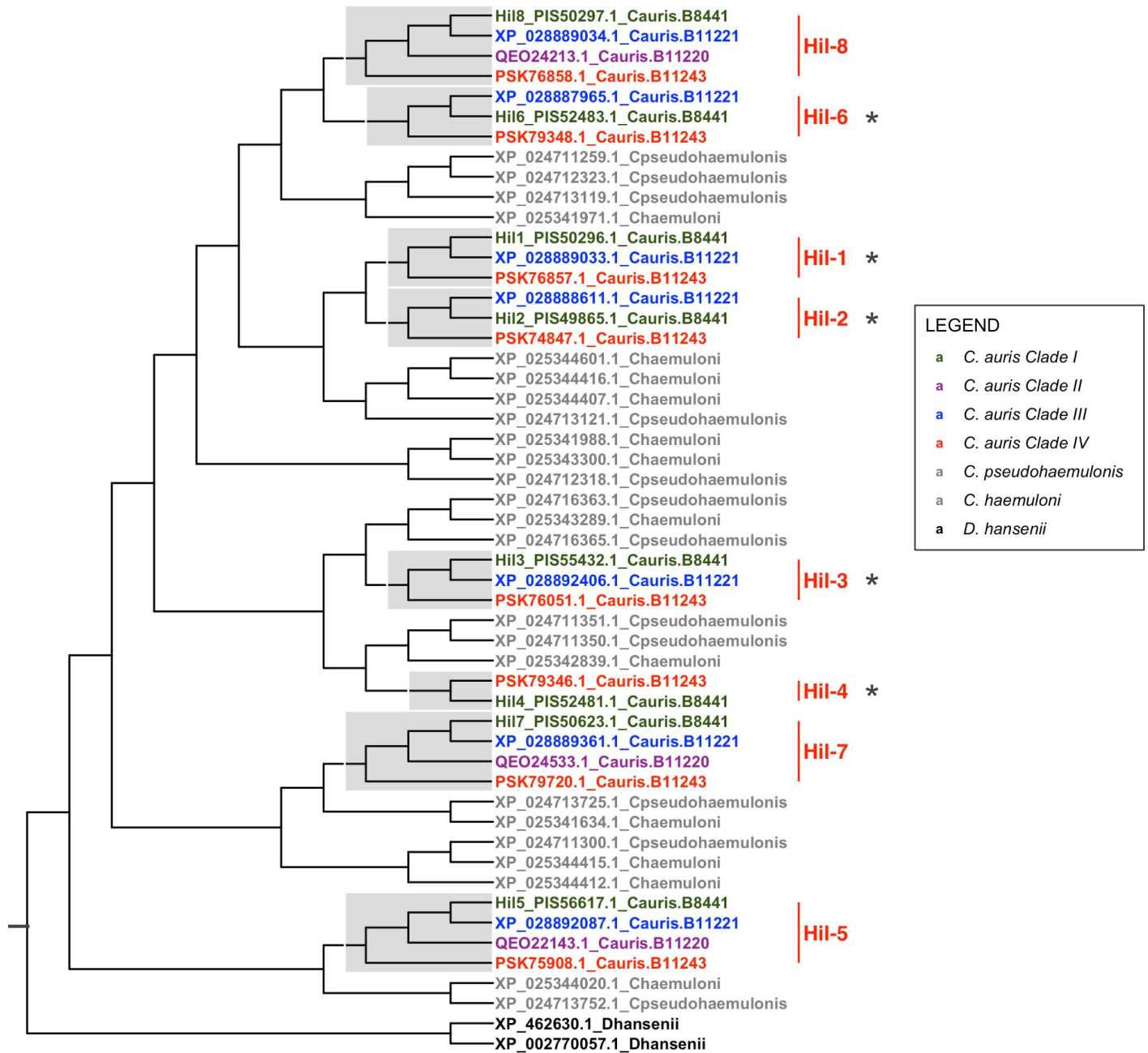
	<b>Hil7</b>	<b>Hil5</b>	<b>Hil3</b>	<b>Hil4</b>	<b>Hil1</b>	<b>Hil2</b>	<b>Hil16</b>	<b>Hil8</b>
<b>Hil7</b>	100	32	36	40	38	41	40	40
<b>Hil5</b>	32	100	41	43	42	44	40	41
<b>Hil3</b>	36	41	100	71	61	62	56	55
<b>Hil4</b>	40	43	71	100	65	67	59	62
<b>Hil1</b>	38	42	61	65	100	83	66	65
<b>Hil2</b>	41	44	62	67	83	100	67	62
<b>Hil6</b>	40	40	56	59	66	67	100	71
<b>Hil8</b>	40	41	55	62	65	62	71	100

**Supplementary figure 4. Percent sequence identity between the PF11765 domains of the eight *C. auris* Hil proteins.** Multiple sequence alignment for the eight PF11765 domain sequences were constructed using Clustal Omega and the percent identity matrix reported by the aligner is reproduced as a heatmap (green = low; yellow = medium; red = high).



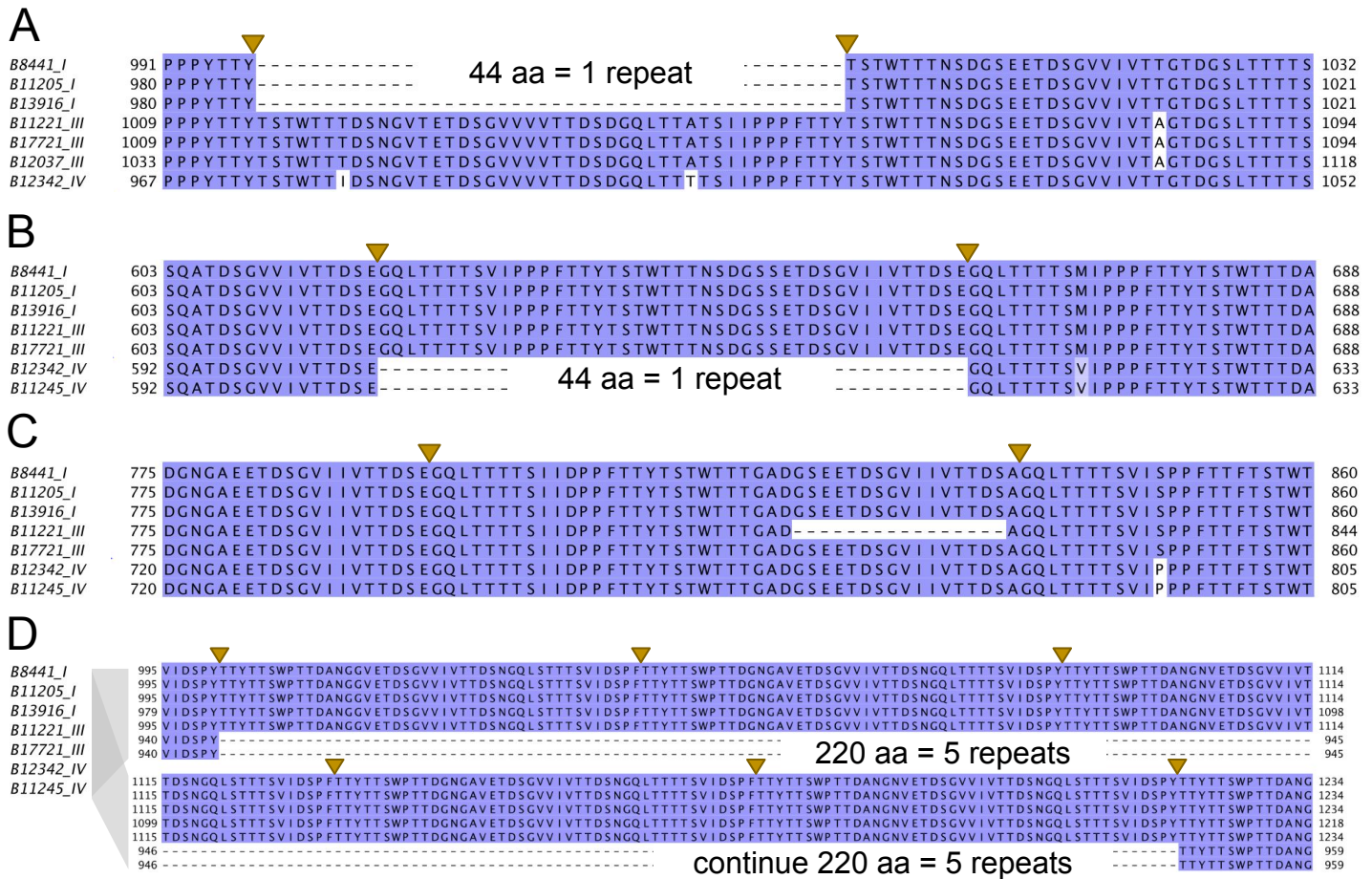


**Supplementary figure 5. Tandem repeats in the *C. auris* Hil1 central domain.** 31 of ~50 tandem repeat copies are shown with a conserved 44 aa period. The remaining copies show similar patterns but are less conserved in length and sequences. Yellow highlights show predicted  $\beta$ -strands by PSIPred; magenta and plum fonts indicate sequences predicted by TANGO to have strong (>90%) or moderate (30-90%)  $\beta$ -aggregation potentials. WebLogo (above) for the pseudo-alignment of the repeats is created by [weblogo.berkeley.edu/logo.cgi](http://weblogo.berkeley.edu/logo.cgi)

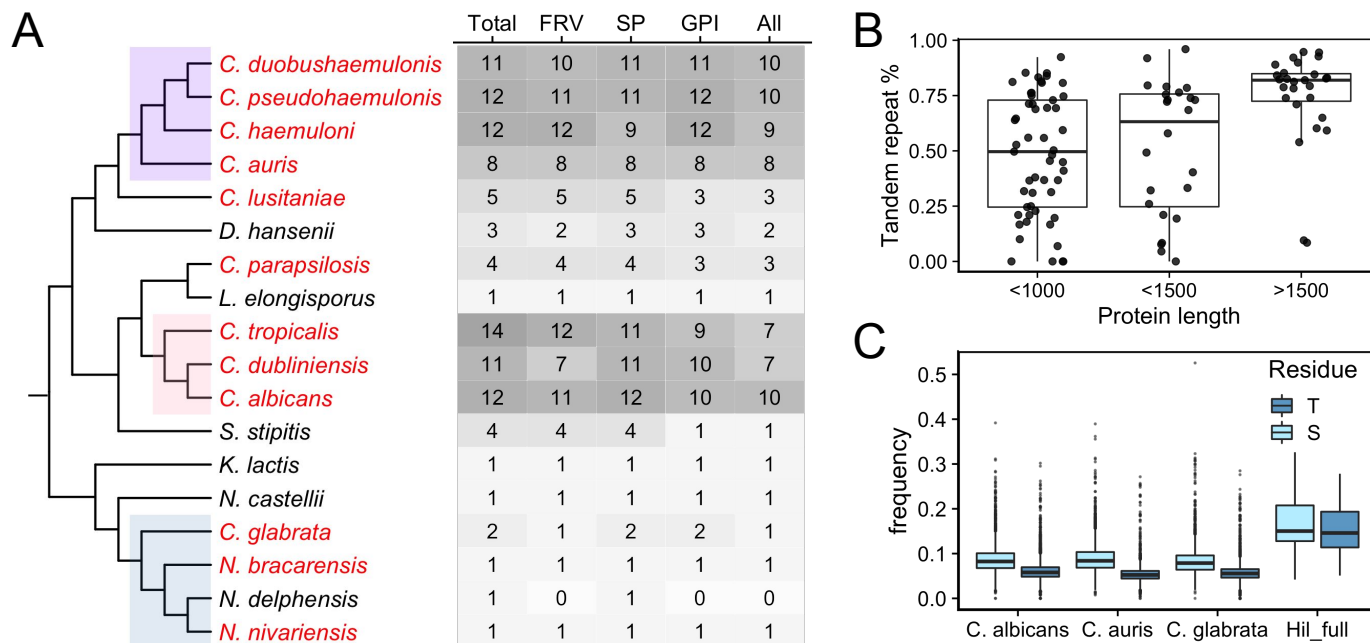


**Supplementary figure 6. Reconciled PF11765 domain tree for the Hil family genes in the four clades of *C. auris* strains and two closely related species.** The tree is rooted by the two homologs from the outgroup *D. hansenii*. The domain tree was reconciled with the species/strain tree based on (Muñoz et al 2018) using GeneRax (v2.0.4). Hil genes lost in *C. auris* Clade II strains are labeled with an asterisk next to the Hil1-8 group labels.

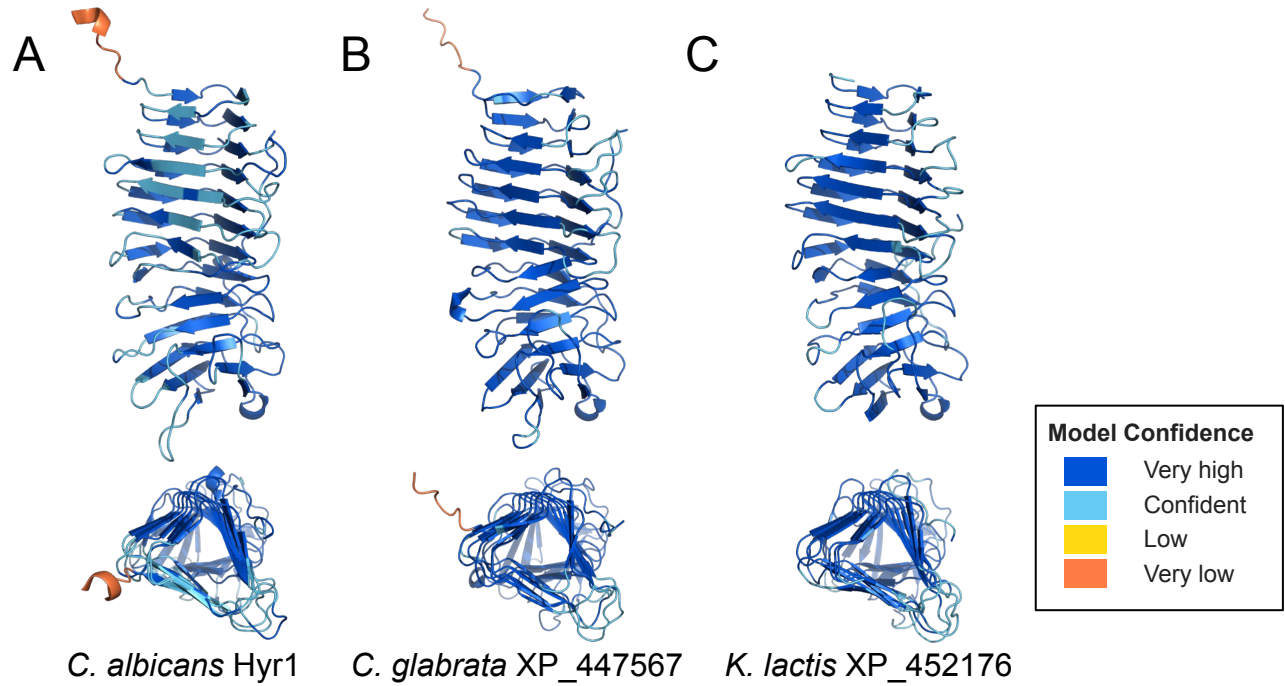




**Supplementary figure 7. Examples of tandem repeat copy number variation in Hil1-Hil4 among the *C. auris* strains.** (A) A 44 aa indel in Hil1 removes exactly one repeat in all three Clade I strain orthologs. (B) A similar indel polymorphism of exactly one repeat length in Hil2 affecting the Clade IV strains. (C) An indel polymorphism in Hil2 that affects one Clade III strain and spans 16 aa, not a full repeat, but includes a predicted strong  $\beta$ -aggregation prone sequence "GVIIVTT". (D) An indel polymorphism in Hil2 that spans 220 aa or five full repeats affecting the Clade IV strains. Similar patterns were observed in Hil3 and Hil4.



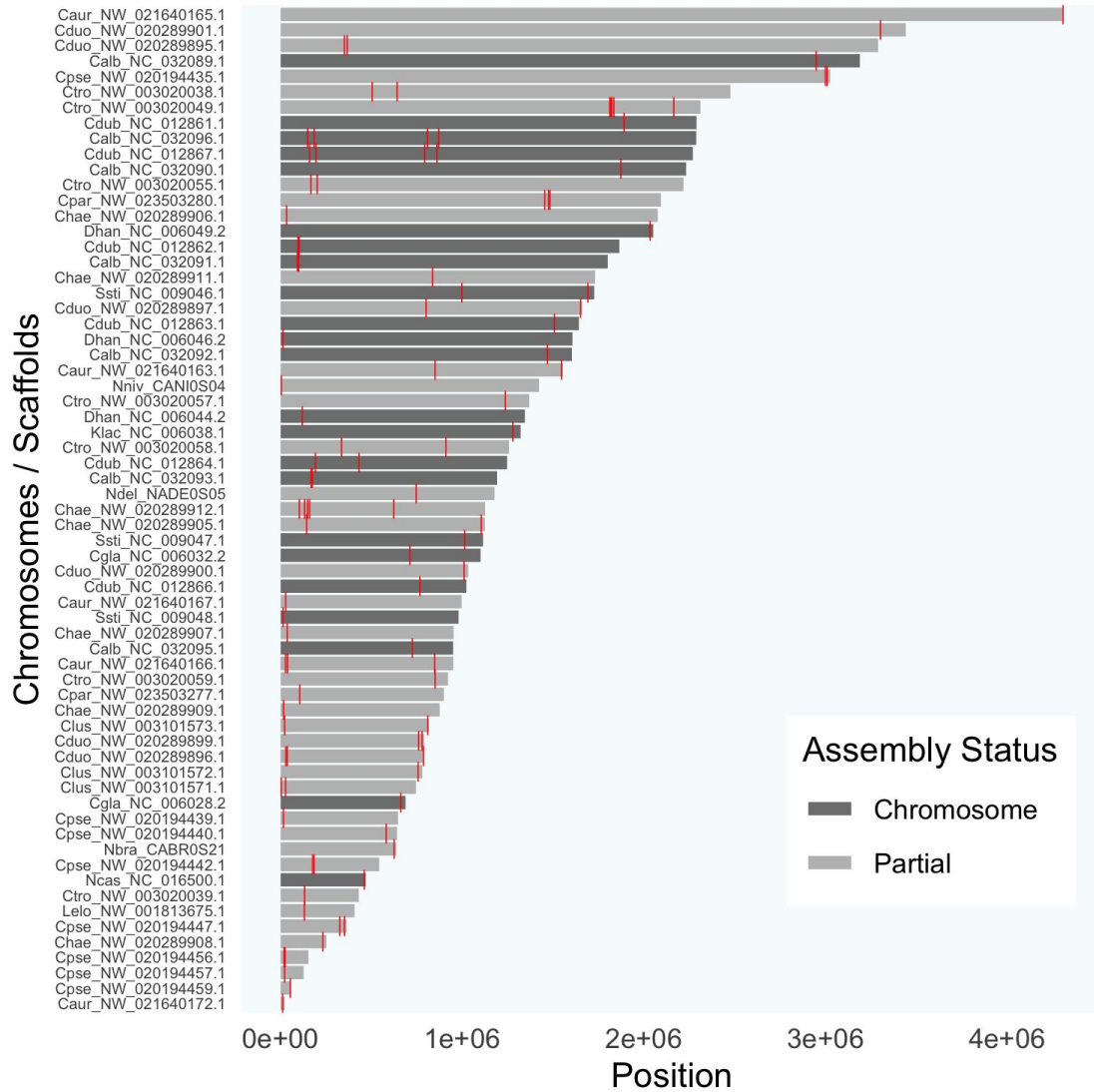
**Supplementary figure 8. Majority of the yeast Hil family genes are likely to encode adhesins.** (A) Species tree with a table showing the total number of Hil family genes and the subset that pass one of the three tests separately and together (All). The three tests are: positive prediction by FungalRV (FRV), signal peptide prediction by SignalP (SP) and GPI-anchor prediction by PredGPI (GPI). (B) Boxplot for the proportion of a protein identified as tandem repeats, excluding the PF11765 domain. The Hil family genes are divided into three groups based on the full protein length. The box shows the interquartile range (IQR); the upper whisker extends to the largest value no further than 1.5 x IQR and similarly for the lower whisker; the middle lines shows the median. Individual proteins are plotted as dots, with their x-values slightly shifted to avoid overplotting. (C) Genome-wide distribution of Thr/Ser frequencies in the entire protein in three species, compared with that in all Hil proteins (Hil\_full). The box plot features are the same as in B except in this case the dots represent outliers beyond the 1.5 x IQR.



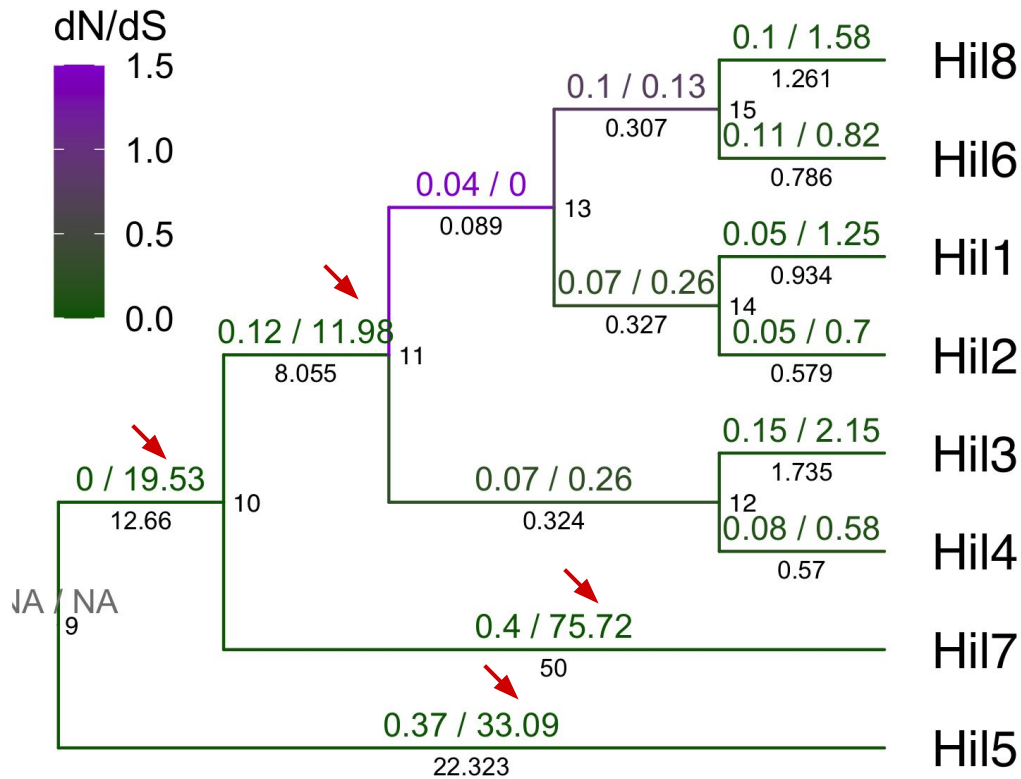
**Supplementary figure 9. AlphaFold2 predicted structures for the PF11765 domain in three distantly related Hil homologs.** The predicted structures are aligned in PyMol and presented in either longitudinal (top) or cross sectional (bottom) view, highlighting the similarities among the three structures made of repeating  $\beta$ -strands forming a superhelix. Panels A, B and C correspond to three Hil proteins from distantly related species as indicated below the cross-sectional view.







**Supplemental figure 11.** Chromosomal locations of the Hil family genes. Each row is either an assembled chromosome (dark grey) or a scaffold (light grey). The length of the bar corresponds to the length of the chromosome or scaffold, whose NCBI IDs are listed on the left. The location of the Hil genes are labeled as red vertical stripes.



**Supplemental figure 12. dN/dS estimates for the PF11765 domain in the *C. auris* Hil family.** Same as Figure 5A except a F3x4 model (“CodonFreq = 2”) instead of F1x4 (“CodonFreq = 1”) was used to estimate the codon frequencies. Also, dN and dS values are labeled on top of all branches to show the unusually high dS estimates on some of them (red arrows). The branch length, defined as the estimated number of substitutions per codon, is labeled under each branch.